

Determination of the Gravitational Constant Using a Beam Balance

Dissertation

zur

Erlangung der naturwissenschaftlichen Doktorwürde

(Dr. sc. nat.)

vorgelegt der

Mathematisch-naturwissenschaftlichen Fakultät

der

Universität Zürich

von

Stephan Schlamminger

aus

Deutschland

Begutachtet von

Prof. Dr. Hugo Keller

Prof. Dr. Walter Kündig

Prof. Dr. Hinrich Meyer

Prof. Dr. Ulrich Straumann

Zürich 2002

Die vorliegende Arbeit wurde von der Mathematisch-naturwissenschaftlichen Fakultät der Universität Zürich auf Antrag von Prof. Dr. Ulrich Straumann und Prof. Dr. Hugo Keller als Dissertation angenommen.

To the memory of

EUGEN HOLZSCHUH († 2001)

ABSTRACT

In this work the Newtonian gravitational constant G was determined with high precision. The constant of gravitation is a measure of the strength of the gravitational interaction. According to the 1998 recommendation of the Committee on Data for Science and Technology (CODATA) the relative uncertainty of this constant is 1500 ppm.

During this work the pervious existing experiment was improved. In this experiment, the gravitational force of two large movable stainless steel vessels, filled with in total 13.5 tons of mercury, changed the weight difference measured on two 1.1 kg masses. The amplitude of this change was determined with a commercially available beam balance.

The starting point of the present work was a determination of G with a relative uncertainty of 220 ppm in 1998. A large part of this uncertainty was caused by a possible nonlinearity of the beam balance. In this work, the influence of this nonlinearity was considerably decreased by means of a new averaging method. Therefore, a special calibration handler was developed. A careful analysis of the data and the experimental error yielded

$$G = 6.674\,07(22) \times 10^{-11} \text{ m}^3 \text{ kg}^{-1} \text{ s}^{-2} .$$

The relative uncertainty of the present measurement is 32.8 ppm. This value is in excellent agreement with most of the values previously obtained with other methods.

ZUSAMMENFASSUNG

In dieser Arbeit wurde die Newtonsche Gravitationskonstante G , welche ein Maß für die Stärke der gravitativen Wechselwirkung darstellt, gemessen. Laut Empfehlung des Committee on Data for Science and Technology (CODATA) 1998 ist die relative Meßunsicherheit dieser Konstanten 1500 ppm.

Ziel der vorliegenden Arbeit war es, ein bereits existierendes Experiment zu verbessern. Die Gravitationskraft von zwei fahrbaren Stahltanks, gefüllt mit insgesamt 13,5 Tonnen Quecksilber, verändert die Gewichts Differenz zweier 1,1 kg Massen. Diese Änderung wurde mit einer kommerziellen Balkenwaage gemessen.

Ausgangspunkt der vorliegenden Arbeit war die Messung von G mit einer relativen Meßunsicherheit von 220 ppm im Jahr 1998. Der größte Beitrag zu dieser Unsicherheit wurde durch eine mögliche Nichtlinearität der Balkenwaage verursacht. Durch ein neues Kompensationsverfahren wurde der Einfluß dieser Nichtlinearität beträchtlich verringert. Dazu wurde eine spezielle Kalibrationsmechanik entwickelt. Eine sorgfältige Analyse der Meßdaten und der experimentellen Unsicherheiten ergab

$$G = 6,674\,07(22) \times 10^{-11} \text{ m}^3 \text{ kg}^{-1} \text{ s}^{-2} .$$

Die relative Unsicherheit dieser Messung ist 32.8 ppm. Dieses Ergebnis stimmt hervorragend mit den meisten bisher veröffentlichten Werten, die ausschließlich mit anderen Methoden gemessen wurden, überein.

CONTENTS

1	Introduction	1
2	The general principle of the experiment	5
2.1	Outline of the experimental setup	5
2.2	Basic ideas of mass integration	6
2.3	Important features of the experiment	9
3	The experimental setup	11
3.1	The field masses	13
3.2	The test masses	18
3.2.1	The copper test masses	18
3.2.2	The tantalum test masses	20
3.2.3	Comparison of the test masses	22
3.3	Surveying the positions	23
3.3.1	Surveying the vertical positions	23
3.3.2	Surveying the horizontal positions	27
3.4	Details of the weighing system	28
3.4.1	Basic properties of the balance	28
	Modification of the balance	29
	Data filtering	30
	Remarks regarding the software	35
	Temperature coefficients	36
3.4.2	Calibration of the balance	38
	The calibration masses	38

	Nonlinear behavior of the balance	41
	The calibration device	43
	3.4.3 The mass exchanger	50
3.5	Controlling the experiment	50
4	Description of the measurement procedure	53
4.1	Auxiliary measurements to characterize the system	53
4.2	Weighing one test mass	57
4.3	One test mass with different loadings	60
4.4	The weight difference	61
4.5	Weight difference for more loadings	62
4.6	The signal amplitude	63
4.7	Calibration	63
4.8	The signal amplitude for more load steps	64
5	Data and their analysis	66
5.1	Calculation of the signal	66
5.2	The amplitude of the signal	68
5.3	Evaluation of the calibration data	69
5.4	Summary of the data	72
6	Practical aspects of the mass integration	75
6.1	Basic equations for the mass integration	75
	6.1.1 The field of a hollow-cylinder	76
	6.1.2 The force on a cylinder	78
	6.1.3 Integration of asymmetric parts	79
6.2	Introduction to automatic differentiation	81
6.3	Results of the mass integration	82
6.4	Uncertainty of the mass integration	83
7	Investigation of the systematic uncertainties	86
7.1	Linearity of the balance	86
	7.1.1 Upper experimental limits	86
	7.1.2 Limits calculated with Monte-Carlo Simu- lations	90
7.2	Sorption Effect	94
7.3	Magnetic forces on the test masses	96
7.4	Position of the test masses	98

7.5	Combination of the uncertainties	99
8	Results and Discussion	102
8.1	The Result of this work	102
8.2	Remarks on the uncertainty budget	103
8.3	The consistency of the results	105
8.4	Comparison with other results	106

LIST OF FIGURES

1.1	The relative uncertainty of fundamental constants.	2
1.2	Measurements of G before 1998	3
2.1	The principle of the experiment.	7
2.2	The gravitational field of one field mass.	8
3.1	A side view of the experiment.	12
3.2	Design of the field mass.	14
3.3	The shape of the top plate of the upper field mass.	15
3.4	A picture of one copper test mass.	19
3.5	A picture of one tantalum test mass.	21
3.6	The measured vertical positions.	24
3.7	The step response of the balance.	32
3.8	The Green's function of the balance.	33
3.9	The autocorrelation of the Green's function.	34
3.10	The transfer function of the balance.	35
3.11	The temperature of balance.	37
3.12	The calibration accuracy at metas.	39
3.13	Illustration of the nonlinearity.	41
3.14	A picture of the wire weights.	45
3.15	Technical drawing of the calibration device.	47
3.16	Sticking of a small wire on the double-stair.	48
3.17	A picture of the calibration device.	49
3.18	Two pictures of the mass suspension.	51

3.19	Load on the balance during mass exchange.	52
4.1	Fourier Transformation of the balance's reading. . .	54
4.2	Oscillation of the balance's reading.	56
4.3	Measurement of one TM. Example of a good fit. . .	59
4.4	Measurement of one TM. Example of a bad fit. . .	60
4.5	A LUL measurement cycle.	61
4.6	Eight ULU or LUL measurements.	62
4.7	A complete TAT measurement.	63
4.8	A complete measurement cycle.	65
5.1	Measured weights for one measurement cycle. . . .	67
5.2	The signal for one measurement cycle.	68
5.3	The signal amplitude for one cycle.	69
5.4	Calibration coefficient.	70
5.5	Difference of CM's.	71
5.6	Results of the measurement series Cu.	73
5.7	Results of the measurement series Ta I.	74
5.8	Results of the measurement series Ta II.	74
6.1	Forces on the test mass.	80
6.2	The influence of tilt and off center parameters. . .	84
7.1	The $\chi^2(\lambda)$ versus λ for the nonlinearity.	88
7.2	The ratio $\frac{\beta}{\alpha}$ versus λ for the nonlinearity.	90
7.3	The remaining error of the nonlinearity (simulation). .	91
7.4	Cumulative percentage of the error.	92
7.5	Temperature change of the vacuum tube.	94
7.6	The magnetic field versus position.	97
7.7	The derivative of the magnetic field.	98
8.1	Comparison of the results from this setup.	105
8.2	Comparison with recent published values	107

LIST OF TABLES

3.1	Comparison of the mercury density.	17
3.2	Technical data of the copper test masses.	19
3.3	The change of the mass of the copper TM's in time.	19
3.4	Technical data of the tantalum test masses.	21
3.5	The change of the mass of the tantalum test masses.	21
3.6	The measured heights.	26
3.7	The position parameters for the final measurements.	27
3.8	The horizontal positions of the test masses.	28
3.9	Overview of the filter characteristic.	36
3.10	The masses of the calibration weights.	40
3.11	Masses of the auxiliary weights.	46
4.1	Technical data of the test mass pendulums.	57
5.1	Overview of the three measurement series.	72
6.1	Subdivision of one field mass.	81
6.2	Results of the mass integration.	83
6.3	The uncertainty budget of the mass integration	85
7.1	Results of the simulations for various scenarios.	93
7.2	Temperature change at the test masses.	95
7.3	The magnetic force on one test mass.	97
7.4	The signal amplitude dependence on position.	99
7.5	The relative uncertainties due to position.	100

7.6	Uncertainty budget of the final result.	101
7.7	Weighted average of the three measurements . . .	101
8.1	Results of the measurement series	103
8.2	Uncertainty budget of the final result.	103

CHAPTER 1

INTRODUCTION

The Newtonian gravitational constant G is a measure of the strength of the gravitational interaction. The attractive force between two point masses m_1 and m_2 separated by the distance r is given by

$$|\vec{F}| = G \frac{m_1 m_2}{r^2} . \quad (1.1)$$

The gravitational constant is one of the first measured fundamental constants of nature¹. The mean density of the earth, equivalent to the gravitational constant, was first determined in 1737-1740 by Bouguer, who observed the change of the period of a second pendulum by the gravitational field of an extensive table-land in Peru. The first measurement in a laboratory was published in 1798 by Henry Cavendish [1].

In spite of this long history of measurement, the current value of G has a large uncertainty. The recommended values of fundamental constants and their uncertainties are published from time to time by the Committee on Data for Science and Technology (CODATA). The last recommendation was made in 1998 [2]. The relative uncertainties of some important fundamental constants of nature as recommended by CODATA in 1998 are shown in Fig. 1.1.

As indicated in Fig. 1.1, the values of these fundamental constants are known with a relative uncertainty of typically 10^{-7} .

¹The speed of light, c , was the first measured constant of nature. It was determined in 1676 by Ole Rømer observing the moons of the Jupiter.

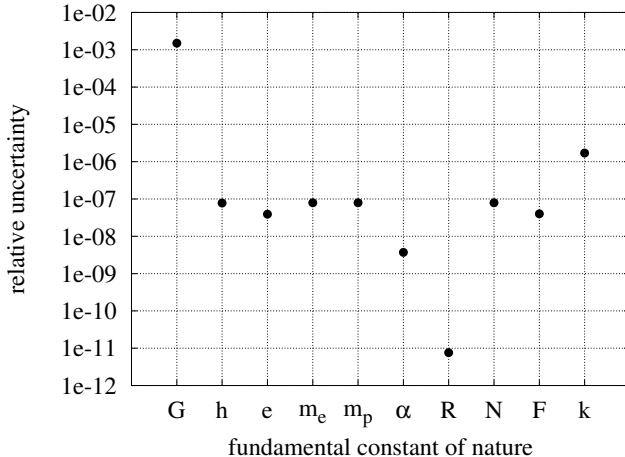


FIGURE 1.1: The relative uncertainty of some fundamental constants as given in the CODATA recommendation of 1998 [2]. The relative uncertainties of the gravitational constant, Planck’s constant, elementary charge, the mass of the electron and the proton, the fine structure constant, the Rydberg constant, Avogadro’s constant, the Faraday’s constant and Boltzmann’s constant are shown.

The relative uncertainty of some constants, such as the Rydberg constant R , are known to a far better precision, namely 10^{-11} . The Newtonian gravitational constant G , however, is only known with a relative uncertainty of 1.5×10^{-3} . This is four orders of magnitude larger than the uncertainties of the majority of the fundamental constants.

Interestingly, the uncertainty of G in the previous CODATA recommendation of 1986 [3] was a factor of 12 smaller. The value was basically the same. Several reasons for this enlargement of the uncertainty of the gravitational constant were given by the CODATA. Three convincing arguments should be noted here. First, a remarkable determination of G was published by a group working at the Physikalisch Technische Bundesanstalt (PTB) in 1996. This result was more than forty standard deviation larger

than the value recommended in 1986 (see Fig. 1.2). Second, even though the experiments were reviewed by several experts, no convincing explanation of the discrepancy has been found up to now. Third, the members of the CODATA wanted the uncertainty to reflect the historical difficulties of the measurement of G , especially the Kuroda effect [4]. This argument needs some additional remarks. The most often used device to measure the gravitational constant has been the horizontal torsion balance. Up till 1995, experimenters considered the torsion constant of the torsion fiber to be independent of the frequency of the torsion pendulum. In 1995, Kuroda showed that this assumption was not valid. Anelasticity in the torsion fiber leads to a frequency dependent torsion coefficient. Depending on the details of the torsion balance experiment, the anelasticity can lead to a systematic bias in the result. Kuroda estimated the order of magnitude for this bias to be 100 ppm.

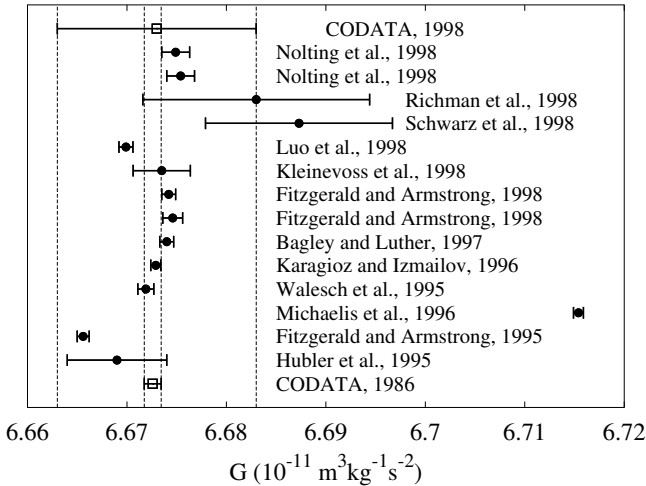


FIGURE 1.2: Measurements [5, 6, 7, 8, 9, 10, 11, 12, 13, 14, 15, 16] of Newton's gravitational constant between the two CODATA recommendations of 1986 [3] and 1998 [2]. The dashed lines show the 1σ uncertainties of the CODATA values.

Summarizing it should be noted, that after 200 years of measurement of the gravitational constant, the situation is very unsatisfactory. The relative uncertainty of the officially recommended value is 1500 ppm. The discovery of the Kuroda effect in 1995 questions the reliability of the torsion balance experiments. The need for a high precision experiment based on a device other than the torsion balance is obvious.

An alternative approach is the experiment described in the present work. A beam balance was used to determine Newton's gravitational constant. The experiment was proposed in 1995 by WALTER KÜNDIG [18]. At this time, the group at the university of Zürich had gained experience with the beam balance in vacuum in a similar experiment performed at the Gigerwald storage lake [5].

A first result of the present experiment was published in 1998 [16, 17, 19, 20]. The relative uncertainty of the published result was 220 ppm. The largest contribution to this uncertainty was a possible nonlinearity of the balance. This contribution was estimated to be 200 ppm. The goal of the work described here was to improve the experiment and to determine a better value for the Newtonian gravitational constant G .

CHAPTER 2

THE GENERAL PRINCIPLE OF THE EXPERIMENT

In this chapter the underlying principle of the experiment is introduced. The ideal case of the experiment without going into technical details and specification of the apparatus is briefly presented.

The general principle of this experiment is identical to the Gigerwald experiment [5]. In that experiment the gravitational force of the water in the Gigerwald storage lake on two test masses was measured. The goal of the experiment was to measure the gravitational constant at an effective distance of approximately 100 m and compare this value with the measurements performed in the laboratory at much smaller distances. The result led to new constraints on the deviation of Newton's gravitation law. However, the accuracy of the experiment could not compete with the laboratory experiment for two reasons. First, the shape of the field generating mass, the lake, was not very well defined. Second the measurement frequency was very low. A complete measurement cycle took one year. Thus, only a few measurement cycles were measured. Consequently the statistical uncertainty was rather large. To overcome these problems, a new experiment was undertaken in the laboratory.

2.1 OUTLINE OF THE EXPERIMENTAL SETUP

The mass setup of the experiment is shown in Fig. 2.1. Two large hollow cylinders, labeled field masses (FM's), can be moved

vertically between the position T (together) and the position A (apart). Two smaller cylinders, called test masses (TM's), can be suspended alternately on the balance. In both field mass positions the signal, defined as the weight difference between the two test masses, is determined. The signal is modulated by changing the field masses between the two positions T and A. The amplitude of this modulation (amplitude of the signal) is used to determine the gravitational constant.

Due to this modulation technique, most of the disturbing forces cancel. The mass difference between the upper and the lower TM, the gravitational gradient and tidal forces vanish, assuming that their change is not correlated with the movement of the FM's. In order to calculate the Newtonian constant of gravitation G , the reading of the balance has to be converted into a force. Therefore, the local acceleration at the position of the pan of the balance is measured. By putting a calibration weight with a known mass on the balance, the reading can be converted into a force.

The symmetric assembly was chosen in order to eliminate many systematic effects. Two TM's were used to cancel out the zero-point drift of the balance. The use of two FM's allowed the position of the field masses to be changed without altering the center of mass. In the present setup, a position correlated tilt was so small, that its effect on the result was of the order of a few parts per million (ppm).

2.2 BASIC IDEAS OF MASS INTEGRATION

The mass integration is a crucial part in all experiments determining G . In order to calculate a value for the gravitational constant the expected force is evaluated for a given value of G . By comparing the calculated force with the measured force, a new value for the gravitational constant can be determined. Experimenters take great pains to keep the mass integration simple and free of errors.

Our experiment was designed to have cylindrical symmetry. In addition, the balance is only sensitive to vertical forces. Both facts simplified the mass integration considerably. For a hollow

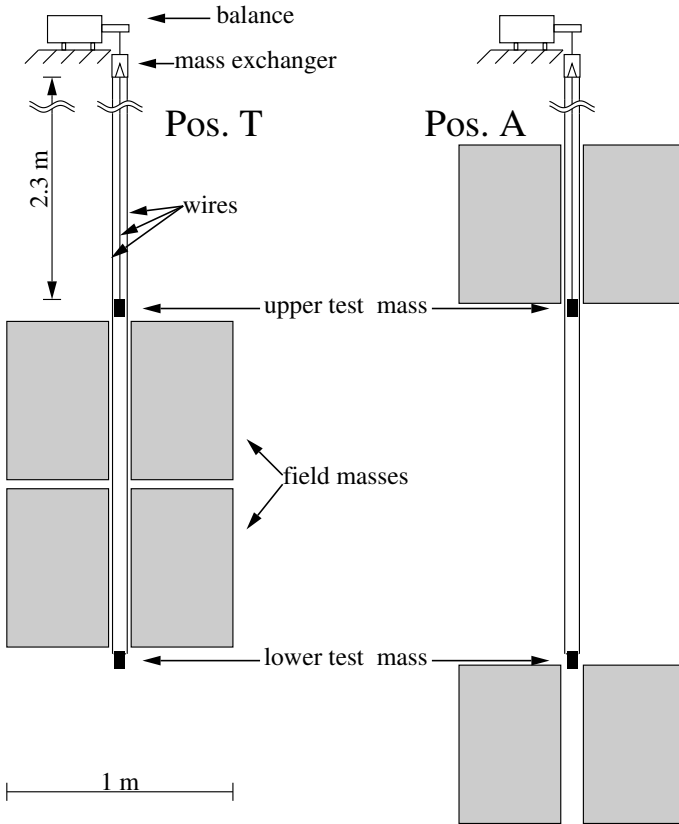


FIGURE 2.1: The principle of the experiment. The two field masses are shown in the two positions together (T) and apart (A) used for the measurements.

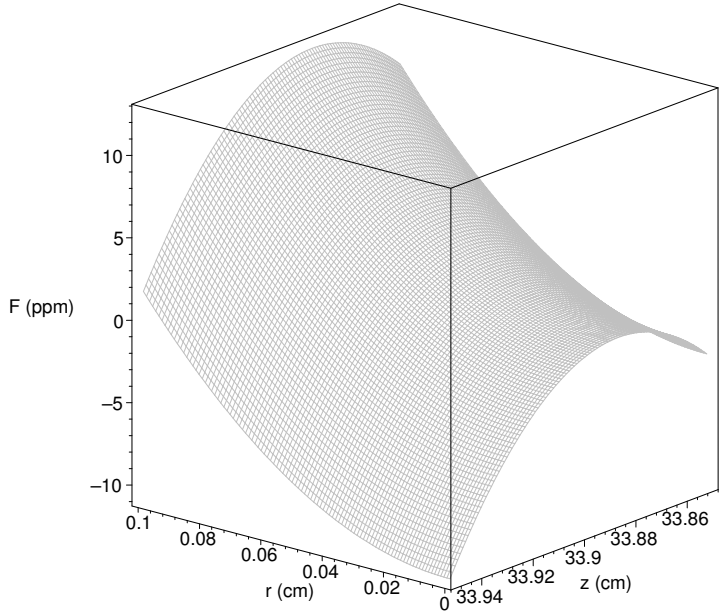


FIGURE 2.2: The gravitational field of one field mass. The deviation of the gravitational field in z-direction g_z from the value at the saddle point. The arrows indicates the order of magnitudes in this plot.

cylinder with density ϱ , height $2B$, inner radius R_1 and outer radius R_2 , the z-component of the gravitational field along the axis of symmetry (z-axis) can be calculated [20] from

$$g_z(0, 0, z) = \frac{\partial \Phi}{\partial z} = 2\pi\varrho G (r_2^+ - r_2^- + r_1^- - r_1^+) , \quad (2.1)$$

with $r_{1,2}^\pm = \sqrt{R_{1,2}^2 + (z \pm B)^2}$.

In Fig. 2.2 the gravitational field in the z-direction g_z of one hollow cylinders with dimensions as used in the experiment is plotted. The gravitational field is a saddle function. There is a maximum in z-direction near the end of the cylinder and a minimum in the r-direction on the axis. Therefore, the force on

a test mass placed at the saddle was, in first order, independent of its position. The accuracy of the metrology of the position between test masses and field masses for a given uncertainty in the result is therefore greatly reduced. As shown in the figure, a position uncertainty of 0.5 mm in both direction would lead to an uncertainty of the order of 20 ppm. For two field masses and two test masses, the situation is more complicated and will be discussed later.

The force in the z -direction on a cylindrical mass m , height $2b$ and radius r in a gravitational field g can be calculated from the expansion

$$F_z = m(g_z + \frac{\partial^2 g_z}{\partial z^2}(\frac{1}{6}b^2 - \frac{1}{8}r^2) + \frac{\partial^4 g_z}{\partial z^4}(\frac{1}{120}b^4 - \frac{1}{48}r^2b^2 + \frac{1}{192}r^4) + \dots) . \quad (2.2)$$

The expansion factors can easily be obtained by integrating the Taylor expansion of a field over the volume of a cylinder. One should note, that the contribution of the second derivative of the field to the total force can be adjusted by changing the factor $b^2/6 - r^2/8$.

2.3 IMPORTANT FEATURES OF THE EXPERIMENT

The most often used device for the measurement of the gravitational constant is the horizontal torsion balance. Our experiment was substantial different in the following points:

- The gravitational force is measured parallel to the local acceleration.
- The gravitational force is measured at an effective distance of 1 m.
- The gravitational force is much larger due to large masses.

Obviously, different approaches have different systematic uncertainties. The experimenters try their very best to identify the

systematic uncertainties and their influence on the result. Nevertheless, some systematic effects may not have been identified.

An example for such a hidden systematic error is the Kuroda effect for the torsion balance discussed in the introduction. The best way to identify such hidden systematic errors is to compare measurements with different basic principles.

Besides the differences relative to torsion balance experiments the following advantages of this experiments should be noted:

- The amplitude of the signal is only slightly sensitive to the positioning of TM and FM.
- Density inhomogeneities are small, since a liquid field mass was used.
- By using different TM's, several consistency checks are possible.
- Many disturbing forces cancel due to the symmetric TM setup (tidal forces, gravitational gradients).
- The tilt effects are considerably reduced due to the symmetric FM setup.
- The mass integration is greatly simplified due to the cylindrical symmetry.
- A high relative accuracy in the dimension metrology is easy to achieve due to the large dimensions.

CHAPTER 3

THE EXPERIMENTAL SETUP

In this chapter a description of the technical details can be found. First an overview of the apparatus is given. After this follows a description of the basic components of the experiment, namely the FM's, the TM's and the balance. A detailed description of the main parts of the experiment can be found in [17]. Thus, in this chapter only the basic features and the major changes are presented.

The experiment was located at the Paul Scherrer Institute (PSI) in Villigen, Switzerland. The apparatus was installed inside a deep pit with thick concrete walls. A side view of the experiment is shown in Fig. 3.1.

The pit was separated by a working platform (10) into two rooms. In the lower room the FM's (14) and the TM's (13,15) were installed. The balance (3), the vacuum system (7), the electronic equipment and the FM drive (8,9) were located in the upper room. Both rooms had their own active temperature stabilization system. The long term temperature stability was better than 0.1 °C. The sensitive parts in the upper room, basically the balance, were mechanically and thermally decoupled from the system in the lower room. The balance was mounted inside a vacuum chamber resting on a granite plate. The granite plate itself lies on two steel girders which were attached to the wall of the pit and not to the working platform. Thus, the balance was mechanically decoupled from the working platform and completely isolated from vibrations of the vacuum pumps. The

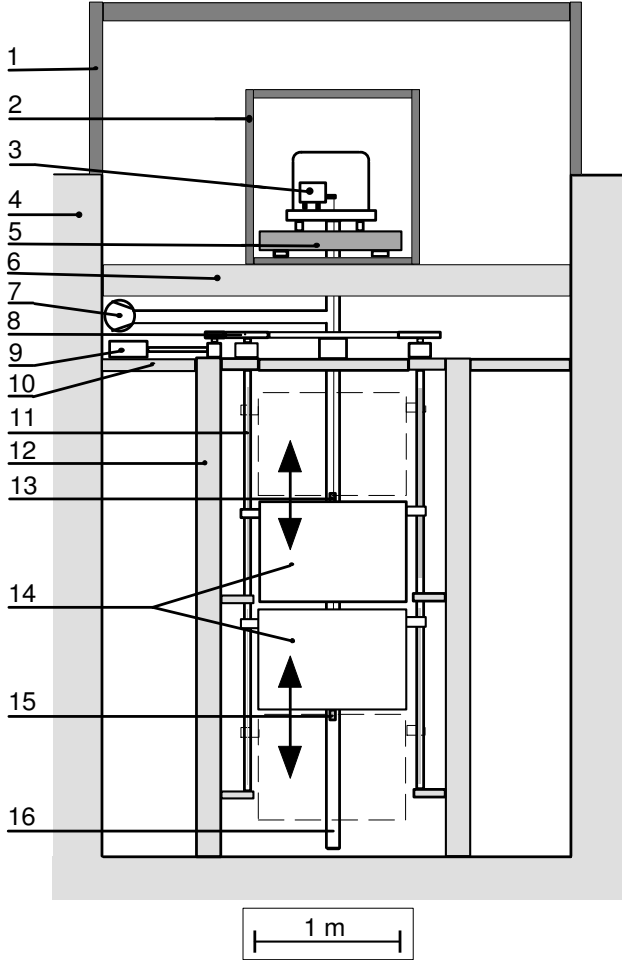


FIGURE 3.1: A side view of the experiment. Legend: 1=chamber, 2=thermally insulated chamber, 3=balance, 4=concrete walls of the pit, 5=granite plate, 6=steel girder, 7=vacuum pumps, 8=gear drive, 9=motor, 10=working platform, 11=spindle, 12=steel girder of the main support, 13=upper TM, 14=FM's, 15=lower TM, 16=vacuum tube.

vacuum system enclosed the balance and the TM's. The vacuum was important in order to avoid convection, buoyancy and other gas pressure forces which would disturb the measurement. The vacuum was 10^{-4} Pa. The vacuum chamber was placed inside a thermally insulated housing (2). In this housing a second active temperature stabilizing system was installed. The long time temperature variation was less than 0.01 °C.

3.1 THE FIELD MASSES

As indicated by the name, the FM's were used to generate a gravitational field which could be measured with the TM's. The FM had a hollow cylindrical shape. The gravitational field of a hollow cylinder is given in Eq. 2.1. The field is proportional to the density of the FM. Thus, in order to get a high field, a high density ρ is necessary. The FM's were stainless steel tanks filled with mercury. A liquid was used, to avoid systematic uncertainties due to density variations. Mercury is the liquid with the highest density at room temperature.

The total volume of the stainless steel tank was 500 l. The outer diameter of the tank was $2R_2 = 1046$ mm, the inner diameter was $2R_1 = 100$ mm and the height of the tank was $2B = 700$ mm. The total mass of one tank, without mercury, was 811.830 kg for the upper and 806.029 kg for the lower tank. To keep the mercury free of air bubbles, the tanks were evacuated before filling with mercury. The mercury mass was determined very carefully by FRITHJOF NOLTING [17]. The total mercury mass in the upper tank was 6 760.017(12) kg and 6 760.618(15) kg for the lower tank.

As shown in Fig. 3.2, one tank was assembled of five basic parts (top and bottom plates, outside casing, central tube and a small compensation vessel). All parts were made of stainless steel and joined together with screws. O-rings were used to seal the vessel. Before the five parts were mounted together, the geometrical dimensions were measured precisely. Especially the central tube of the tank was machined and measured very carefully. The inner diameter of the cylinder was ground and honed. A maximum diameter variation less than 10 μ m was achieved. The

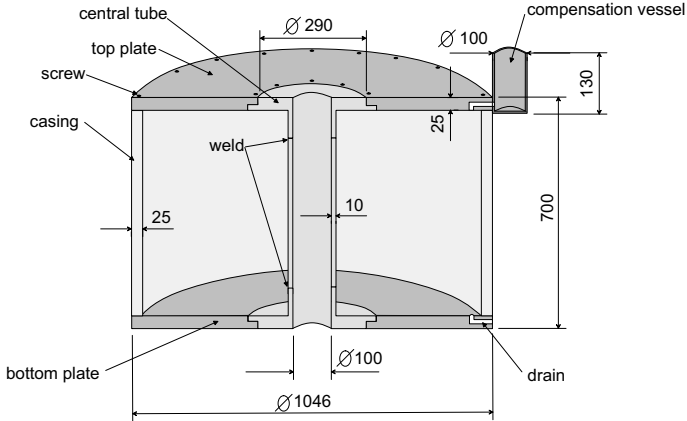


FIGURE 3.2: Design of the field mass. All dimensions are given in mm.

diameter was measured with an accuracy of $1 \mu\text{m}$. The measurements were made by an external company [21] at 20°C .

For the mass integration the measured coordinates had to be corrected for the thermal expansion. The ambient temperature at the experiment was between 21.18°C and 21.27°C . A linear thermal expansion coefficient $\alpha_{SS} = 16.0 \times 10^{-6} \text{ K}^{-1}$ [22] was used to scale the coordinates.

The filling of the tanks with mercury slightly changed the shape of the tanks. Especially the top and bottom plates were bent. The shapes of the filled tanks were measured with a laser tracker [23]. This device measured the absolute distance with a laser interferometer and the horizontal and vertical angle with two angular encoder. The absolute accuracy in the distance measurement was 0.025 mm. The accuracy of the angle measurement was 0.005 mm/m. The absolute determination of the height of each tank was made with an accuracy of 0.05 mm. The shape of the top and the bottom plates has been measured with much higher accuracy (typically 0.005 mm). A typical measurement, that of the top plate of the upper tank, is shown in Fig. 3.3. For the mass integration, the shapes measured with the laser tracker combined with the thickness measurements of the individual parts

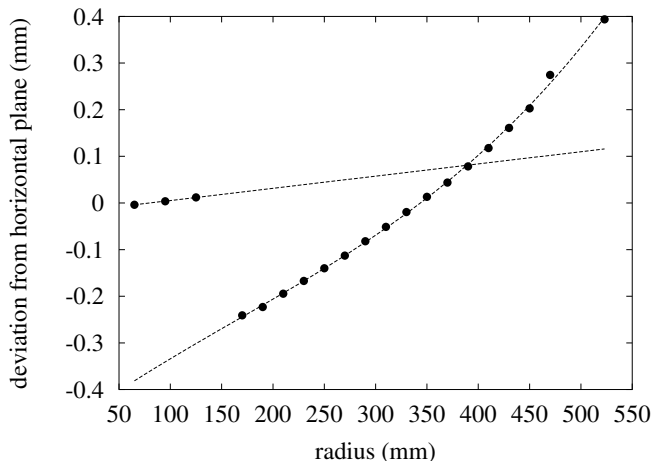


FIGURE 3.3: The shape of the top plate of the upper field mass. In the figure, the deviation from the horizontal plane is shown as a function of radius. The step at 150 mm occurred due to the interface of the central tube and the top casing. The two lines are fitted polynomial functions used to describe the shape for the mass integration.

before mounting the tank were used.

The geometrical dimensions of both tanks were precisely determined. Thus, the mercury volume of the tanks could be calculated. The only other dimension necessary to determine the mercury volume was the height of mercury in the compensation vessels. In both compensation vessels, level indicators were mounted. The readout of the level indicator was fully computer controlled.

During the filling of the tanks with mercury, several mercury samples were taken. The density of these samples was measured at the Physikalisch Technische Bundesanstalt (PTB), Braunschweig. At a temperature of 20 °C and a pressure of 10 1325 Pa, a mercury density of 13 545.89(04) kg/m³ for the samples from the upper field mass and 13 545.95(04) kg/m³ for the samples from the lower field mass was obtained [24]. Both val-

ues are very close to the value 13 545.848(7) kg/m³ given in [25].

The mercury density had to be corrected for the ambient temperature and the pressure. Therefore, the equation

$$\varrho(T) = \frac{\varrho_{20}}{a + bT + cT^2 + dT^3 + eT^4} \quad (3.1)$$

with

$$\begin{aligned} a &= 9.963\,79 \times 10^{-1}, \\ b &= 1.809\,29 \times 10^{-4}, \\ c &= 5.438\,54 \times 10^{-9}, \\ d &= 3.485\,33 \times 10^{-11} \text{ and} \\ e &= 1.550\,17 \times 10^{-14} \end{aligned}$$

was used [25]. The temperature in °C is denoted by T .

Due to the hydrostatic pressure of approximately 700 mm mercury, a linearized pressure correction had to be applied. The mean density of the mercury in the vessels was 1.90(2) ppm higher than the density of the mercury under normal pressure. The relative density gradient across the height of the vessel was twice as large.

The corrected density values were compared to the density obtained from the measured mass and geometrical determined volume. See Table 3.1 for this comparison.

The relative uncertainty of the PTB-values was 3 ppm. The relative uncertainty of the mass measurement was 1.8 ppm for the upper and 2.2 ppm for the lower tank. The relative uncertainty in the volume determination of both tanks was 10 ppm. Thus, the relative uncertainty for the density obtained by mass and volume was 10.2. The difference between the densities obtained by the two methods was 6.4 ppm and 1.8 ppm for the upper and lower FM. They agreed well within the uncertainty of the difference (10.6 ppm). Both the volume determination and the mass integration were based on the same geometrical data of the tanks. An error in the dimension data would have led to a different mercury volume and thus density. The agreement of the densities obtained by the two methods ruled out such an error.

Nr.	series	upper field mass		density PTB (kg/m ³)	difference (ppm)	lower field mass		density PTB (kg/m ³)	difference (ppm)
		temp- erature (°C)	density geometrical (kg/m ³)			temp- erature (°C)	density geometrical (kg/m ³)		
1	Cu	21.180	13 542.93	13 543.02	−6.6	21.282	13 542.80	13 542.83	−2.2
2	Cu	21.188	13 542.91	13 543.00	−6.6	21.281	13 542.80	13 542.83	−2.2
3	Cu	21.192	13 542.91	13 542.99	−5.9	21.282	13 542.80	13 542.83	−2.2
4	Ta-I	21.212	13 542.86	13 542.94	−5.9	21.226	13 542.98	13 542.97	−0.7
5	Ta-I	21.233	13 542.79	13 542.89	−7.4	21.243	13 542.96	13 542.93	−2.2
6	Ta-I	21.228	13 542.80	13 542.90	−7.4	21.238	13 542.96	13 542.94	−1.5
7	Ta-I	21.226	13 542.80	13 542.91	−8.1	21.239	13 542.96	13 542.94	−1.5
8	Ta-I	21.237	13 542.79	13 542.88	−6.6	21.242	13 542.96	13 542.93	−2.2
9	Ta-II	21.264	13 542.73	13 542.81	−5.9	21.255	13 542.89	13 542.90	−0.7
10	Ta-II	21.274	13 542.71	13 542.79	−5.9	21.266	13 542.90	13 542.87	−2.2
mean					−6.4				
standard deviation					1.2				

TABLE 3.1: Comparison of the mercury densities. For both tanks, the density determined by the mass of the mercury and the volume given by the dimension metrology is compared to the density based on the values determined by the PTB.

As shown in Table 3.1 the standard deviation of the difference was of the order of 1 ppm. This measurement uncertainty consisted of two parts, namely the uncertainty of the temperature determination and the uncertainty of the mercury height in the compensation vessel.

3.2 THE TEST MASSES

The TM were brought into the gravitational field of the FM's and the force acting on them was measured. Two different sets of TM's have been used in order to check systematic uncertainties. The first set of TM's was constructed by FRITHJOF NOLTING. They were made of copper. The other TM's were made of tantalum.

3.2.1 *The copper test masses*

The average density for the copper was $\varrho_{Cu} = 8927.4 \text{ kg/m}^3$. An upper limit for the density variation was $\Delta\varrho_{Cu}/\varrho_{Cu} = 2 \times 10^{-4}$. The measured susceptibility of the copper was $\chi = +4 \times 10^{-6}$. The diameter of one TM was $2r \simeq 45 \text{ mm}$ and the height $2b \simeq 77 \text{ mm}$. The mass of one copper TM was $m \simeq 1096 \text{ g}$. The accurate geometric dimensions are listed in Table 3.2. They were measured with a coordinate measuring machine (CMM) at PSI. In order to prevent oxidation of the copper, the TM's were gold plated. Each copper TM was suspended with two tungsten wires on the mass exchanger. The supporting wires were looped around two cylindrical lugs which were pressed into diametrical blind holes in the upper part of the TM's. The lugs themselves were made of Cu-Be (BERYLCO-25). Figure 3.4 shows a picture of one copper TM.

The mass of the TM's were determined before and after each measurement. These determinations were made by MARKETA MALINA from *Mettler Toledo*. The results of the measurements are shown in Table 3.3. The variation of the mass during five years was less than $440 \mu\text{g}$. This corresponds to a relative change in the mass of 0.4 ppm which is negligible for this experiment.

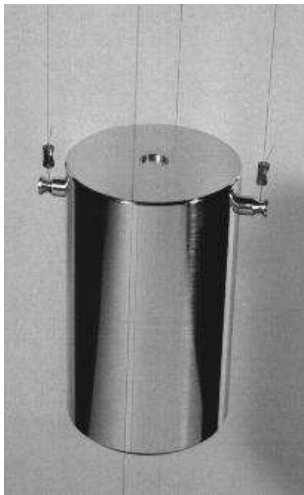


FIGURE 3.4: A picture of one copper test mass. The wires with the small crimping tubes support this mass at two lugs. The other two wires run to the lower test mass which is not shown here.

	diameter $2r$ (mm)	height $2b$ (mm)	mass m (g)
upper	45.045(5)	77.066(5)	1 097.606 9(3)
lower	45.039(5)	76.884(5)	1 095.073 3(3)

TABLE 3.2: Technical data of the copper test masses.

date	mass upper TM (g)	mass lower TM (g)
10th May 1996	1 097.607 15(25)	1 095.073 48(25)
3rd December 1996	1 097.606 97(25)	1 095.073 41(25)
4th December 1996	1 097.606 94(25)	1 095.073 37(25)
5th September 1997	1 097.607 03(25)	1 095.073 47(25)
9th November 1998	1 097.607 02(25)	1 095.073 37(25)
23rd December 1999	1 097.606 71(25)	1 095.073 19(25)
15th December 2000	1 097.607 11(25)	1 095.073 50(25)
10th December 2001	1 097.606 94(25)	1 095.073 33(25)

TABLE 3.3: The change of the mass of the copper TM's in time.

One wants to keep the mass difference between the upper and the lower TM together with the suspension devices within the amplitude of the signal ($780\text{ }\mu\text{g}$). Therefore, a small copper ring was placed on the lower mass for fine trimming. The inner diameter of the ring was $3.7(1)\text{ mm}$, the outer diameter $5.944(4)\text{ mm}$, the height $1.068(8)\text{ mm}$ and the mass $158.38(2)\text{ mg}$.

3.2.2 *The tantalum test masses*

The density of tantalum is almost a factor two higher than that of copper. Thus, the tantalum TM's were much more compact. The total height of one TM was $2b \simeq 40\text{ mm}$ and the diameter $2r \simeq 45.8\text{ mm}$. The mass was close to the mass of one copper TM. The precise technical data of the tantalum TM's are shown in Table 3.4. These values were also measured with the CMM at PSI. A picture of one tantalum TM is shown in Fig. 3.5.

Both the density and magnetic susceptibility were determined by PHILIPPE RICHARD from metas. The measured susceptibility was $\chi = +1.90(7) \times 10^{-4}$. The mean value for the density was $\rho_{Ta} = 16\,662(5)\text{ kg/m}^3$. The relative density variation was smaller than $\Delta\rho_{Ta}/\rho_{Ta} = 1 \times 10^{-3}$.

To fine trim the mass difference between the upper and the lower TM a small ring made of tantalum was placed on the lower TM. The dimensions of this ring were the following: outer diameter $4.993(1)\text{ mm}$, inner diameter $3.00(1)\text{ mm}$, height $2.112(3)\text{ mm}$ and the mass $436.66(2)\text{ mg}$. Tantalum has a very thin and stable natural surface oxide layer similar to that of aluminum. Thus, the TM's were not gold plated.

The masses of the TM's were measured before and after use in the experiment. The results of these measurements are shown in Table 3.5. Both TM's had gained a small amount of mass ($440\text{ }\mu\text{g}$). This was an indication, that the surface area had not stabilized after the manufacturing process. Nevertheless, the total gain in mass was below 0.5 ppm and therefore negligible.

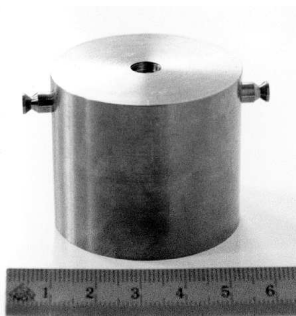


FIGURE 3.5: A picture of one tantalum test mass.

	diameter $2r$ (mm)	height $2b$ (mm)	mass m (g)
upper	45.801(10)	39.899(3)	1 097.606 9(3)
lower	45.814(10)	39.790(5)	1 095.073 3(3)

TABLE 3.4: Technical data of the tantalum test masses.

date	mass upper TM (g)	mass lower TM (g)
27th November 2001	1 097.488 36(25)	1 094.673 02(25)
29th May 2002	1 097.488 72(25)	1 094.673 46(25)

TABLE 3.5: The change of the mass of the tantalum test masses.

3.2.3 Comparison of the test masses

The reason for the measurement with the tantalum TM's is given in Eq. 2.2. The largest contribution to the gravitational force in the axial direction (z) of a cylinder in a field is given by the product of the mass of the cylinder and the field mg_z . The second term is the product of the second derivative of the field times in the z-direction times the geometric factor $b^2/6 - r^2/8$. By choosing $b = \sqrt{3}/2r$, the contribution of the second derivative to the force vanishes. It was neither possible to use a diameter larger than 46 mm, because of geometrical limitations, nor to change the mass of the TM by more than 0.5 g, because of the weighing range of the balance (see section 3.4.1). Thus, the only way to achieve a smaller geometric factor was to increase the density of the TM's. By employing tantalum TM's, the geometric factor was reduced by a factor of 230.

Measurements with both sets of TM's allowed important consistency checks. As mentioned above, the numerical mass integration had different contributions of the derivatives of the field in the z-direction. Inconsistent results for the gravitational constant for the different TM's would be an indication of an erroneous mass integration.

Systematic effects due to water sorption on the TM's depend basically on the surface properties of the masses. The magnitude of this effect was given by the surface area of the TM's. The time constant was given by the heat transfer to the TM. Dominated by radiation, the heat transfer depends on the reflectivity of the mass. Both factors were significantly different for tantalum and copper. First, the surface area of the tantalum TM was just half that of the copper TM. Second, the surface of the copper TM was highly reflective due to the gold layer, whereas the surface of the tantalum TM was dark gray.

The third physical quantity that differed for both sets of TM's was the magnetic susceptibility. The value of the tantalum pieces was a factor of 50 larger than that of the copper pieces. The magnetic forces on the tantalum TM's are 25 times larger due to their smaller volume. A detailed discussion of all three effects can be found in section 7.3.

3.3 SURVEYING THE POSITIONS

In the previous two sections the detailed technical data of the FM's and the TM's were discussed. Even more important than the internal measures of these masses were the relations between them. The positions of FM's and TM's were measured with a leveling instrument and a theodolite. A great assistance for these measurements was provided by the surveying group of the Paul Scherrer Institute ULRICH FELLMAN and JEAN-LUC POCHON.

A leveling instrument is basically a telescope, which is carefully adjusted to be in horizontal plane with the help of a very accurate water level. The telescope can be rotated in this plane. Thus, it is possible to read markings on a scale placed on different objects and thereby compare their heights. The heights were measured with respect to a post mounted on the floor of the experiment. The height of a object could be measured in respect to this post with an uncertainty of 0.035 mm [26] for a single reading.

The theodolite [27] was a commercial theodolite from *Leica*. The working distance inside the pit was much smaller (1.5 m) than the distances for which the theodolite was built. Thus, a correction lens was needed. Consequently, the systematic uncertainty of the theodolite was somewhat greater than the quoted accuracy of the device. The off-center position of the TM could be measured with an uncertainty of 0.1 mm.

3.3.1 *Surveying the vertical positions*

With the help of the leveling instruments different heights on the experiments were measured with respect to the post defining the origin 00 (see Fig. 3.6). To ensure a well defined measurement of the FM position, they were measured on the top or bottom surface at position close to the inner diameter. According to Fig. 3.3 the deformation of the tanks at this position is small (typically below 0.01 mm). The TM's were measured on the top surface. The TM's were machined carefully on a lathe, so this surface was well defined (0.01 mm).

It was possible to position the leveling instrument accurately

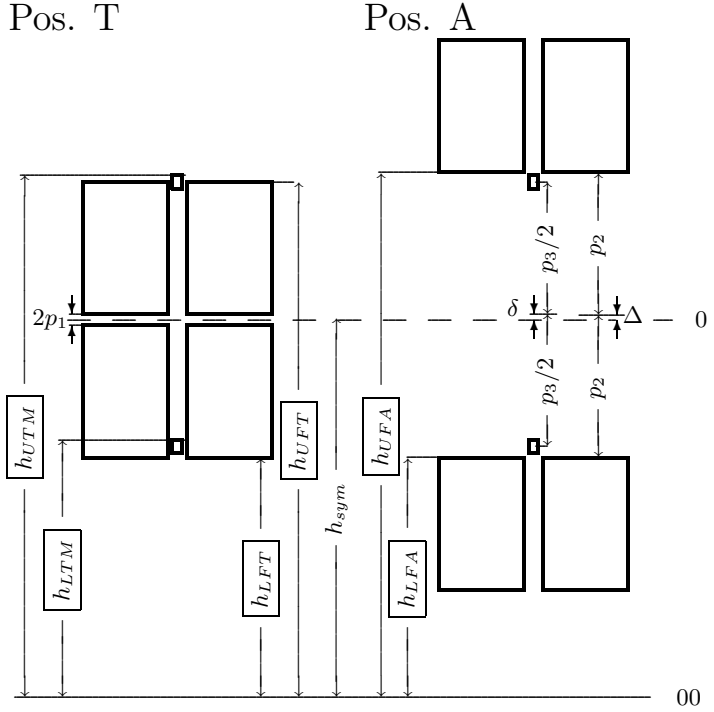


FIGURE 3.6: The vertical dimensions of the experiment. The six variables surrounded by boxes represent the measured heights relative to the origin 00. The resulting six parameters were used for the calculation of the gravitational constant. The dashed line labeled 0 gives the symmetry axis of the experiment. It was defined to be in the middle of both field masses in position T.

on four different mounting brackets at the experimental site. Due to this, the following heights with respect to 00 could be measured. In position T, the bottom side of the lower tank h_{LFT} and the top side of the upper tank h_{UFT} ; in position A, the top side of the lower tank h_{LFA} and the bottom side of the upper tank h_{UFA} . In addition, the top surface of the TM's were measured (h_{UTM}, h_{LTM}). These six measurements along with the dimensions of the TM's and FM's were used to determine the six parameters $p_1, p_2, p_3, \Delta, \delta$ and h_{sym} shown in Fig. 3.6. The calculation of the gravitational constant was made with these parameters. The parameters Δ and δ were small asymmetry parameters relative to ideal positions. The parameters p_1, p_2 and p_3 were the half distances between the FM's in both positions and distance between the centers of the TM's. The parameter h_{sym} gave the height of the symmetry plane 0 of the experiment above 00. This parameter was not needed for the calculation of the gravitational constant.

To perform the measurements with the leveling device, the vacuum tube has to be open. Various measurements showed that due to evacuation, the lower flange of the vacuum chamber was bent. Thus, the vertical position of the balance changed slightly and both TM's moved downwards. This variation was measured a few times and found to be $\epsilon_p = 0.10(3)$ mm. The asymmetry parameter δ has been corrected by this amount.

The measurements with the leveling instrument were performed before and after each measurement series. In addition, the positions of the FM's were continuously monitored with two digital length-difference instruments [28]. The zero-points of these instruments were arbitrary fixed. Thus, the driving distance of the FM's and the reproducibility of the tank movements could be observed. The uncertainty for both was 0.014 mm. The measured tank positions always agreed within this uncertainty. The results measured with the leveling instruments and with the digital instruments were combined using a least-square fit.

The values for the six parameters as used in the final measurements are shown in Table 3.7. Two things are remarkable. First, the asymmetry of the FM's was in all cases the same $\Delta = 0.052$ mm. This asymmetry is given by the imperfection of

No	date	h_{UFA} (mm)	h_{UTM} (mm)	h_{UFT} (mm)	h_{LFT} (mm)	h_{LTM} (mm)	h_{LFA} (mm)	TM
1	1st Sep. 97	2 545.65	2 537.09	2 452.65	1 042.69	1 034.44	949.68	Cu
2	23rd Sep. 97	2 461.18	2 495.68	2 452.63	1 042.66	1 077.15	1 034.05	Cu
3	21st Jan. 98	2 461.28	2 495.62	2 451.50	1 042.07	1 076.90	1 033.52	Cu
4	17th Mar. 98	2 460.13	2 495.58	2 451.47	1 042.06	1 077.02	1 033.52	Cu
5	26th Oct. 98	2 460.09	2 495.62	2 451.52	1 042.06	1 077.05	1 033.54	Cu
6	16th Dec. 98	2 460.12	2 495.62	2 451.50	1 041.94	1 077.08	1 033.42	Cu
7	3rd Nov. 99	2 460.10	2 495.42	2 451.51	1 042.07	1 076.85	1 033.51	Cu
9	14th Mar. 00	2 460.10	2 495.43	2 451.42	1 042.01	1 077.11	1 033.47	Cu
10	8th May 01	2 460.21	2 495.34	2 451.55	1 042.01	1 076.97	1 033.47	Cu
11	13th Nov. 01	2 460.15	2 495.23	2 451.57	1 042.00	1 076.89	1 033.48	Cu
12	12th Dec. 01	2 475.59	2 485.62	2 453.04	1 040.46	1 047.82	1 018.11	Ta
13	14th May 02	2 475.51	2 485.48	2 453.06	1 040.47	1 047.63	1 018.04	Ta

TABLE 3.6: The heights measured with the leveling instrument.

meas.	p_1 (mm)	p_2 (mm)	p_3 (mm)	Δ (mm)	δ (mm)	h_{sym} (mm)
Cu	4.269	713.355	1 418.269	0.052	0.750	1 746.773
Ta I	5.789	728.735	1 437.766	0.052	-0.135	1 746.753
Ta II	4.269	713.355	1 437.766	0.052	-0.135	1 746.773

TABLE 3.7: The position parameters for the final measurements. In total, three different mass setups were measured, labeled Cu, Ta I and Ta II. For the Ta II measurement the TM position is the same as that of the Ta I measurement, whereas the FM position is the same as that of the Cu measurement.

the spindles on which the FM's were mounted. Second, the height of the zero-line h_{sym} differs by only 0.02 mm. This is within the measurement uncertainty. Both facts illustrate the consistency of the vertical position measurements.

The surveying of the vertical position of the TM also involved a measurement of the tilt of the TM. The tilt was determined by measuring the height of the upper surface of the TM at two diametrically opposite points. It was found that the maximum tilt angle of the TM was less than 0.017 rad. This was sufficiently accurate for our purpose.

3.3.2 Surveying the horizontal positions

The horizontal position of the TM was surveyed with a theodolite. As shown in Fig. 2.2, the gravitational force indicates only a small dependence on the distance from the symmetry axis. The uncertainty of the measurement with the theodolite was 0.1 mm. The deviation from the axis was measured along two almost orthogonal directions. The measured values can be found in Table 3.8. The interesting columns are δ_{RUT} and δ_{RLT} , describing the distance between the axis of the upper and the lower TM from the axis of the experiment.

No.	δ_{XUT} (mm)	δ_{YUT} (mm)	δ_{RUT} (mm)	δ_{XLT} (mm)	δ_{YLT} (mm)	δ_{RLT} (mm)	TM
1	-0.14	0.01	0.14	0.23	0.57	0.61	Cu
2	0.32	0.43	0.54	0.24	0.48	0.54	Cu
4	0.42	0.40	0.58	0.36	0.58	0.68	Cu
5	0.40	0.40	0.57	0.32	0.56	0.65	Cu
6	-0.10	-0.21	0.23	0.13	0.37	0.39	Cu
7	-0.09	-0.23	0.25	0.13	0.30	0.33	Cu
9	0.82	0.52	0.97	0.04	-0.30	0.30	Cu
10	-0.35	-0.17	0.39	0.09	0.50	0.51	Cu
11	-0.48	0.10	0.49	0.01	0.52	0.52	Cu
12	-0.22	-0.20	0.30	0.01	0.20	0.20	Ta
13	-0.14	-0.23	0.27	0.06	0.09	0.11	Ta

TABLE 3.8: The horizontal positions of the test masses.

3.4 DETAILS OF THE WEIGHING SYSTEM

The most important part of the experiment was the weighing system. It can be divided in three parts, namely the balance, the mass suspension and the calibration device. The balance was used to measure the gravitational force on the TM's. With the mass suspension, one of the two TM's was connected to the balance. It allowed a smooth exchange of the connection from one TM to the other. The calibration device was used to calibrate the balance and to compensate for a possible nonlinearity of the balance.

3.4.1 *Basic properties of the balance*

The gravitational force was measured with a single-arm beam balance. It was a modified *Mettler-Toledo* AT1006 mass comparator. A detailed description of the balance can be found in the thesis of FRITHJOF NOLTING [17]. The main part of the load was balanced by a counterweight mounted on the beam. A smaller part was compensated by an electromagnetic system. This system consisted of a coil mounted on the beam and a permanent magnet mounted on the balance's frame. An electrical current was driven through the coil such that the beam remained in the horizontal position. The position of the beam was measured by an optical system. The electrical current was digitized by the

electronic circuitry of the balance and displayed after some digital data processing. The balance was additionally equipped with a parallelogram guide. This made the reading of the balance to first order independent of the load position.

MODIFICATION OF THE BALANCE

After the measurement performed by FRITHJOF NOLTING and JÜRGEN SCHURR in 1997 and 1998, the balance was modified. In particular, the coil mounted on the beam was replaced. The new coil had a factor of six fewer turns. This reduced the weighing range of the balance from 24 g to 4 g. A reliable linear reading was only possible within a range of 1.5 g. This range was called the electrical range. In order to avoid errors, the software of the balance only gave an output within this range.

The main reason for decreasing the number of turn was to increase the resolution. Obviously the current required to compensate a given weight, for example 1 g, was increased by a factor of six and therefore the least significant bit in the analog to digital converter (ADC) had a higher resolution in terms of grams. The price paid for the higher resolution was a higher current in the coil which led to increased resistance heating in the coil. Since the balance was placed in the vacuum, the amount of heat was troublesome. The heating could have been avoided by using thicker wires for the turns of the coil. It turned out, however, that the larger part of the resistance was due to the feed lines. The coil was connected by two small gold bands (thickness 0.010(1) mm, width 0.23(2) mm and length 33(3) mm). Both bands together had a resistance of 2.86 Ω ; the coil resistance was 0.24 Ω . With the Stefan–Boltzmann law of thermal radiation, the temperature in vacuum for these connection bands was calculated. At the working point of the balance, the temperature of the bands was 5 K higher than the ambient temperature. A change of weight of 100 mg increased the temperature another 2.2 K. The time constant for this rise was calculated to be 200 s. Unfortunately the connection bands were not changed when the coil was replaced. Connections with a higher cross section have less resistance. Consequently the heating could have been reduced. On the other

hand, thicker connections would apply a greater torque to the beam. Since the connection wires were mechanically attached to the beam and to the frame of the balance, they produce a torque on the beam. Fortunately, the beam remains at the same position and this torque should cancel out when two measurements are compared. Nevertheless, a high torque should be avoided. Consequently, a trade-off between resistance heating and torque had to be made. The connection wires were not changed. Nevertheless, from the experience gained in this experiment, I would strongly recommend thicker connection wires when the balance is operated in vacuum. To overcome the problems due to self heating of the balance, care was taken in the measurement procedure. Especially, load changes were kept small in order to avoid thermal gradients at the beam of the balance.

The balance modification was carried out at the *metrotec* company by MARTIN BAUMELER. He also changed the suspension of the beam and the parallelogram guide. The thickness of the flexure strips was decreased by a factor of two. In addition the complete balance was cleaned and the balance software was upgraded. With the new software, the resolution of the values shown at the balance's display was 12.5 ng compared with 100 ng before the improvement.

DATA FILTERING

Apart from the excellent mechanical part of the balance, the data reduction was designed very carefully by *Mettler Toledo*. Unfortunately, neither a complete documentation nor the source code of the software for the microprocessor in the balance was available. Therefore, a considerable part of the balance had to be treated as a black box. To investigate the behavior of the balance, several experiments were performed.

The balance was connected to the serial port of a personal computer. The balance sent the readings continuously to the computer. The time between two successive readings was exactly 0.3788 s. The timing by counting the reading was much more precise than the timer of the computer. For the following investigation of the behavior of the balance in the time domain, an

accurate measurement of time was important. Thus, the reading of the balance was used for timing. In contrast, during the normal operation of the experiment, timing was not a critical factor and the clock of the computer was used.

Users of a *Mettler-Toldeo* mass comparator have the possibility to influence the display by selecting different options. In this work, a large number of options were turned off. Only two options were of interest.

The first option was called range (abbreviated by RG). The values fine (F) and coarse (C) were possible. In the coarse mode, the last digit was not displayed. For the balance used here, the resolution in the fine mode was 12.5 ng and 125 ng in the coarse mode.

The second option was called vibration adapter (abbreviation: MI), with filter ranges 1,2 and 3. By changing this parameter, the cutoff frequency of the low-pass filter in the balance was changed.

To investigate the balance behavior for different settings, the step response of the balance was recorded. A 1 g wire weight was put on the balance with a step motor driven handler and the balance's readings were recorded. The result of these measurements are shown in Fig. 3.7.

The first derivative of the step response is the Green's function. The Green's function is the response of a linear system to a delta function excitation. The behavior of a linear system is completely determined by its Green's function. The Green's function of the balance is shown for the filter setting (RG F, MI 3) in Fig. 3.8.

From the Green's function, valuable information can be obtained. In Fig. 3.9 the autocorrelation function of the Green's function is shown. This function shows that after an excitation of the balance, it takes about 20 s until the reading of the balance is no longer correlated with the previous reading. In order to get a valid reading it was necessary to wait at least this 20 s. In addition, it was sufficient to take just one reading because subsequent readings were highly correlated and contained no additional information. The correlation between successive readings had another consequence for the data analysis. When fitting a function to correlated data with the method of the least squares,

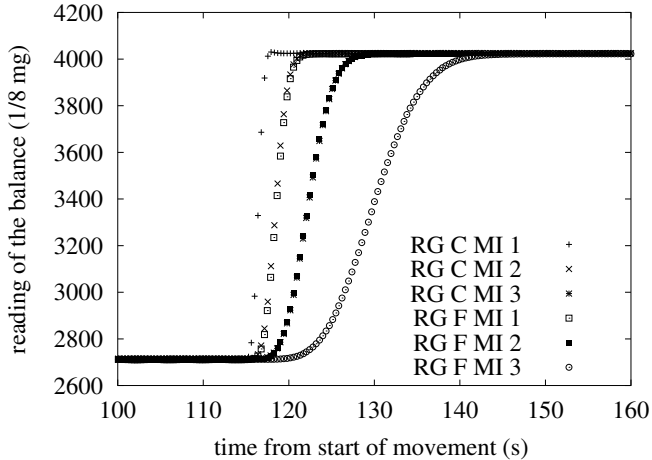


FIGURE 3.7: The reading of the balance vs. time after loading the balance partly with a 1 g wire weight. The response was recorded for the three settings (1,2,3) for the vibration adapter (MI) and for the two different range (RG) settings, coarse(C) and fine(F).

the correlation has to be taken into account. Usually this is done by calculating the χ^2 with the inverse of the covariance matrix. Unfortunately it was not possible to invert the covariance matrix as determined from the autocorrelation function. Numerical instabilities led to a singular matrix. Thus, the least square fits of the balance readings were always made without taking the correlation into account. Although the correlation were not taken into account, the values differ only slightly from the best values. However, the expectation of the χ^2 is no longer the number of degrees of freedom. More details on fitting functions to the balance readings can be found in section 4.2.

The frequency dependence of a linear device is given by a Fourier transformation of the Green's function. This function is called the transfer function. For the *Mettler-Toledo* AT-1006 the transfer function is shown in Fig. 3.10. Imagine that the balance was excited by a sinusoidal force with a given amplitude. The

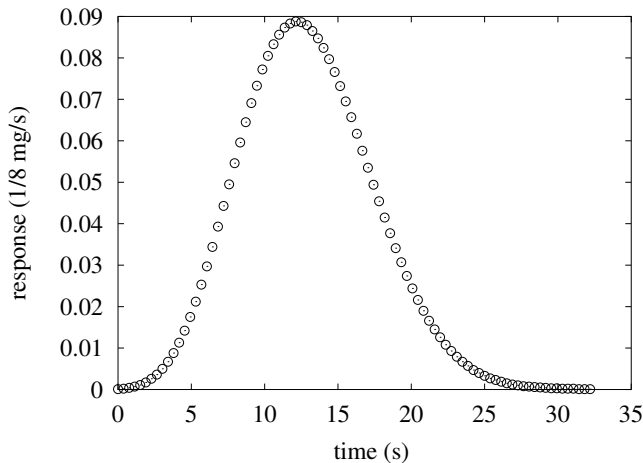


FIGURE 3.8: The Green's function of the balance gives of the system in time to a delta-peak at time zero. This function is the derivative of the step response shifted in time. The function displayed here was measured for RG F, MI 3. The function is normalized such that the total area is $1/8$ mg.

transfer function gives the amplitude of the sinusoidal output of the balance as a function of the frequency. The function is normalized such that it has the value one for zero frequency. The frequency transfer of the balance was due partly to the weighing system. The main characteristics, however, were caused by the software filters. The software filters had a strong low-pass characteristic. The slope of the line fitted to some data points in Fig. 3.10 indicates a ν^{-8} behavior for frequencies in the range of 0.06 Hz – 0.13 Hz. Thus, the software filter in the balance was of 4th order. A more detailed analysis of the transfer function showed that a Bessel type low-pass filter was used. The cutoff angular frequency for this filter was $\omega_l = 0.2 \text{ s}^{-1}$. Cutoff frequency refers to the frequency at half amplitude in the transfer function.

In the Fig. 3.8-3.10 only data for one filter setting (RG F, MI 3) are shown. In this mode, the balance showed the longest

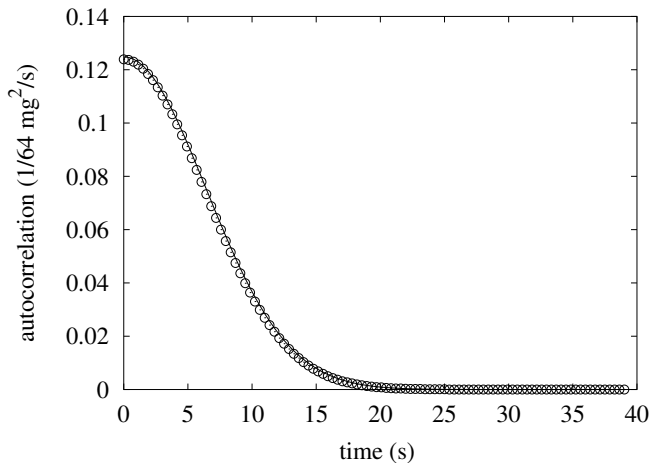


FIGURE 3.9: The autocorrelation function of the Green's function. The solid line is a Gaussian fit. The standard deviation obtained by the fit was 6.391(14) s. The function shown is normalized.

time constant. The plots were much nicer to present because they were much smoother and contained more data points. Nevertheless, the analysis was performed for all six possible settings. An overview of the results are given in Table 3.9. The cutoff frequency could be changed by a factor of two for different settings. The other features such as the width of the Green's function, the width of the correlation function and the cutoff frequency scales accordingly. The scaling showed a very precise behavior as indicated in Table 3.9.

For the measurement, the highest possible resolution and the fastest response of the balance were desired. The balance was used with the RG F MI 1 setting. Thus, the cutoff frequency was $\omega_l = 0.8 \text{ s}^{-1}$ and the width of the correlation function was $\sigma_C = 1.53 \text{ s}$. It is sufficient to wait about eight σ_C , approximately 12 s, after a load change before reading the balance. To make sure that the data were completely uncorrelated with the pervious measurement data were taken 40 s after a load change.

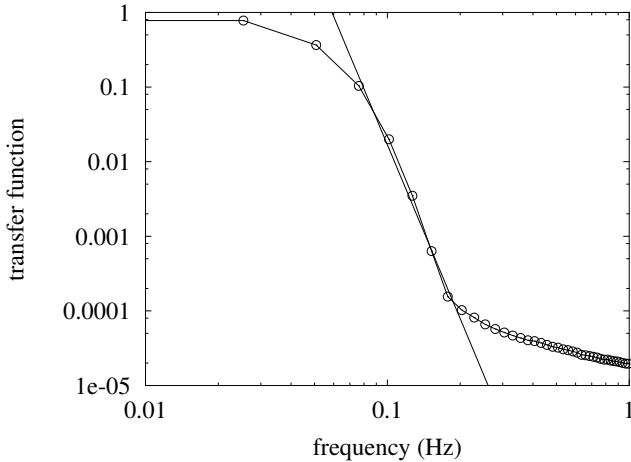


FIGURE 3.10: The transfer function of the balance. For a sinusoidal excitation of the balance, the transfer function gives the amplitude of the balance's output as a function of the frequency. The transfer function is normalized (has the value one for zero frequency). The solid lines indicates a ν^{-8} behavior.

REMARKS REGARDING THE SOFTWARE

As mentioned above, the commercial version of the balance has a lot of user friendly options. In the balance used for this work, a special balance software was used. In this software all these options were turned off. In addition the reading of the balance was given as a six byte, hexadecimal number without units. The corresponding resolution of this number was 12.5 ng. Furthermore, a second, faster weighing mode was available. In this mode, the balance gave a reading every 4.2 ms with a lower resolution. The total mechanical range of the balance (4 g) was covered with one byte. Thus, the resolution was 15.6 mg. This mode was used for the exchange of the TM's (see section 3.4.3).

filter setting		ω_l (s ⁻¹)	$\omega_l \tau_G$	$\omega_l \sigma_G$	$\omega_l \sigma_C$
RG C	MI 1	1.6	3.010	0.906	1.278
RG C	MI 2	0.8	2.998	0.856	1.207
RG C	MI 3	0.4	3.002	0.891	1.260
RG F	MI 1	0.8	2.999	0.865	1.224
RG F	MI 2	0.4	3.003	0.890	1.259
RG F	MI 3	0.2	3.003	0.892	1.278

TABLE 3.9: Four properties of the software filter in the balance. All parameters were determined experimentally. To show the precision of the scaling, the mean of the Green’s function τ_G , the broadness of the Green’s function σ_G and the broadness of the correlation function σ_C are multiplied with the cutoff frequency ω_l .

TEMPERATURE COEFFICIENTS

The reading of every balance is influenced by two essential temperature coefficients. The first describes the variation of the zero-point with temperature. The second describes the dependence of the sensitivity. The sensitivity is the change of the reading of the balance due to the addition of a small mass, divided by the small mass. The calibration coefficient c_c , the inverse of the sensitivity is given by the ratio of the mass put on the balance and the change in reading. The reading multiplied with the calibration coefficient is known as the calibrated reading.

Both temperature coefficients were measured. The coefficient for the zero-point drift was determined to be $TK_{zero} = 5.5$ mg/K. For the temperature dependence of the sensitivity, the value $TK_{sens} = 224 \times 10^{-6}$ K⁻¹ was obtained. This value can be explained by the temperature coefficient of the permanent magnet. The permanent magnet was made from AlNiCo 5-7. The temperature coefficient of the magnetization is approximately 200×10^{-6} K⁻¹. The much larger temperature coefficient for the zero-point can be explained by temperature induced change of the lever ratios [29]. Comparable balances showed similar values for the zero-point drift.

Basically, the zero-point drift of the balance did not affect the result of the experiment. The measured signal was the difference of the reading for the upper and the lower TM. By using a three-fold ABA measurement (see section 4.4) a linear zero-point drift of the balance can be suppressed. To ensure a smooth variation of the balance's temperature, the balance was mounted inside a large copper box. The total mass of 45 kg copper and its large heat capacity 17 kJ/K led to a stable temperature of the balance. The large heat capacity (capacitor) and the vacuum around the balance (resistor) acted like a low-pass filter for incoming temperature variations. The temperature of the balance was stable within 1 mK. A measurement of the balance temperature is shown in Fig. 3.11.

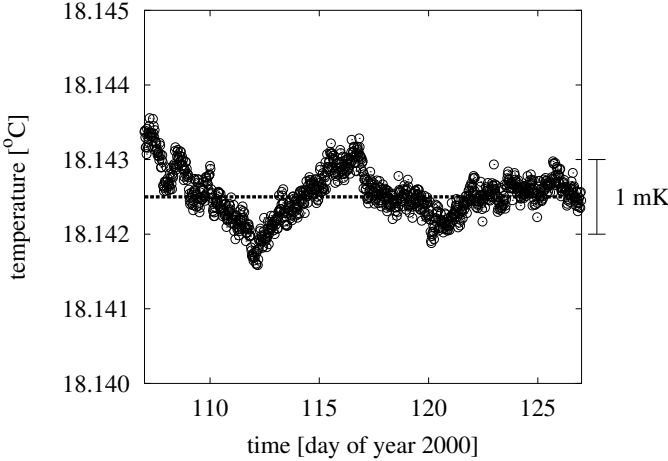


FIGURE 3.11: The temperature of the balance versus time. In this plot data of 20 days of measurement made in year 2000 are shown. The absolute value of the temperature in this plot is not calibrated.

A change of the sensitivity of the balance did affect the measurement. To minimize this effect, the balance was calibrated periodically. The sensitivity change of the balance was monitored and canceled by applying the measured calibration coefficients.

3.4.2 Calibration of the balance

In order to calibrate a balance, a weight with known mass must be measured. By dividing the mass by the reading of the balance a calibration coefficient c_c can be established.

The determination of the calibration coefficient was only the first part of the calibration for this experiment. To determine the gravitational constant, the force on the TM has to be measured. Thus, the reading of the balance had to be converted into a force. This was done by multiplying the calibrated reading of the balance with the value of the local acceleration at the balance pan. The local acceleration was measured [17]. The value was $g = 9.807\,233\,5(6) \text{ m/s}^2$.

THE CALIBRATION MASSES

The mass of the calibration weight should be close to the measured signal. Obviously, without that condition a scaling error might effect the calibration. Unfortunately, the relative uncertainty to which the mass of a weight can be determined increases significantly with decreasing mass (see Fig. 3.12). The kg is defined as the mass of the international prototype of the kilogram. Obviously the kg is the quantity of mass that can be measured with the highest precision, by comparing it to the international prototype. For smaller masses, say 100 g weights, the relative uncertainty increases. This is due to the fact that besides the measuring of ten 100 g weights together, intercomparisons must be made in order to obtain the individual values. Each intercomparison contributes an uncertainty to this determination. The absolute uncertainty for smaller masses is at least as large as the absolute uncertainty for the 1 kg masses. Consequently, due to the smaller mass, the relative uncertainty is higher.

A compromise for the mass of the calibration weight had to be made. First, it should be close to the amplitude of the signal (0.8 mg) and second, the relative uncertainty of the mass determination should be lower than 10 ppm. The best choice was to take a 200 mg calibration weight. This mass can be calibrated with a relative uncertainty of 4 ppm, but it was a factor of 250 larger than the amplitude of our signal. The second condition

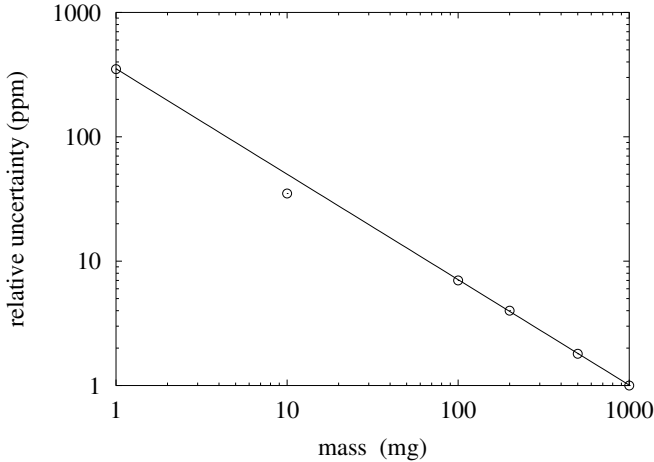


FIGURE 3.12: The relative uncertainty of a mass determination at the Swiss national metrology institute metas versus the mass [35]. By using a more careful method the 100 mg mass had been calibrated with an uncertainty of 3.5 ppm. The solid line was obtained by a fit to the four right points.

was fulfilled but the first was not. To minimize the scaling error a special method described below was developed.

In practice two calibration masses (CM's) of 100 mg instead of a single 200 mg mass were used. This redundancy made the calibration safer and allowed further investigations. In a dusty environment the mass of a wire can change by $1 \mu\text{g}$ by accumulating dust. This is already 10 ppm for a 100 mg weight. By using two calibration weights such a change in mass can be monitored.

Two calibration weights allowed the investigation of another effect. The calibration of the wire weights was performed at metas in ambient air. In the experiment, the CM's were used to calibrate the balance in vacuum. A thin water sorption layer would affect the calibration process. This effect could be determined by using two calibration wires with different surface areas. The two calibration weights (see Fig. 3.14) were labeled CM-2 and

CM-14. Both were made of stainless steel wires. The density of a sample of the wires was measured by metas. The density was found to be $\varrho = 8008 \text{ kg/m}^3$. The diameter of the wire for the CM-2 was 0.96(1) mm; that of the CM-14 was 0.50(1) mm. Both CM's had approximately the same mass, 100.3 mg. Thus, the surface area of the CM-14 was a factor 1.92 larger than that of the CM-2. The sorption effect would therefore differ by the same factor for both calibration weights. Nevertheless, comparing both weights in vacuum and in air, a significant sorption effect on the calibration masses was never observed.

The CM's were sent to metas for calibration three times. The results of the calibration are shown in Table 3.10. It turned out, that the mass of CM-2 changed irreversible between the two measurements. Additional data indicated, that the change in mass occurred during the second trip to metas (Bern). It was believed, that a dust particle was responsible for this change in mass. The particle was removed during the second trip to Bern. The diameter of a spherical aluminum particle ($\varrho = 2700 \text{ kg/m}^3$) with a mass of $1 \text{ } \mu\text{g}$ is 0.09 mm. Even though this particle should have been visible to the naked eye, it is reasonable to assume that it was overlooked.

According to PHILIPPE RICHARD the measurement uncertainties of the masses of CM-2 and CM-14 were correlated. Thus, the difference and the sum of the masses could only be calculated with an uncertainty of $0.8 \text{ } \mu\text{g}$ or $0.7 \text{ } \mu\text{g}$ respectively. Both numbers were considered in the uncertainty budget.

date	mass of CM-2 (mg)	mass of CM-14 (mg)
6th February 2001	100.263 90(40)	100.270 30(40)
29th November 2002	100.262 90(35)	100.270 20(35)
27th May 2002	100.262 97(35)	100.270 01(35)

TABLE 3.10: The masses of the calibration weights as determined at metas.

NONLINEAR BEHAVIOR OF THE BALANCE

For the reason explained above, the mass of the two CM's together (200 mg) was a factor of 250 larger than the amplitude of the signal (0.8 mg). The question arose, whether the calibration coefficient of the balance is constant over a range of two orders of magnitude.

The effect of a nonlinear behavior of the balance is illustrated in Fig. 3.13. At the working point, the sensitivity of the balance might be different for the small signal than for the large calibration weight. Consequently a scaling error, referred to as nonlinearity error, may occur. It was impossible to measure the nonlinearity of the balance with sufficient precision in a reasonable time. Only some consistency checks could be made. For example, both calibration weights were measured with the balance and compared with the sum of the individual measurements. No nonlinearity within the measurement uncertainty (300 ng) was found. This corresponds to 3 ppm of the calibration weight, but is 380 ppm of the signal. This obviously did not solve the problem.

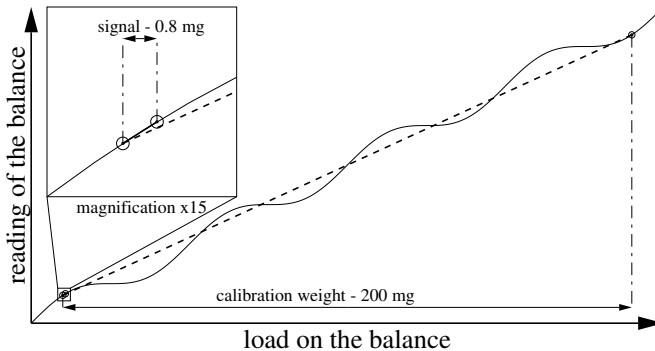


FIGURE 3.13: Illustration of the nonlinearity of the balance as a function of load. For clarity the nonlinearity is greatly exaggerated.

One way to get rid of nonlinearities of any system is the following: Instead of measuring the signal at one working point, the

signal is measured at many working points within the calibration range. By averaging the measured signals, the nonlinearity cancels. The explanation for this is given below.

Let $f(x)$ denote the response of a nonlinear system and s is the unknown signal that should be measured with that system. The working point is given by a and the calibration range is given by c with $b = a + c$. Thus, the calibration coefficient of the system can be obtained from $c_c = (b - a)/(f(b) - f(a))$. A basic formula in calculus gives

$$\int_a^b \frac{df}{dx}(x') dx' = f(b) - f(a) . \quad (3.2)$$

The integral can be approximated by a sum, and the derivative by a difference, which results in

$$\int_a^b \frac{df}{dx}(x') dx' \approx \frac{b-a}{N} \sum_{i=0}^{N-1} \frac{f(x_i + s) - f(x_i)}{s} , \quad (3.3)$$

where $x_i = a + i\delta$ and $\delta = (b-a)/N$. By multiplying the combined equation by $s/(f(b) - f(a))$ one obtains

$$s \approx c_c \frac{1}{N} \sum_{i=0}^{N-1} f(x_i + s) - f(x_i) . \quad (3.4)$$

Two approximations were used in this derivation. First, the integral is approximated by the sum

$$\int_a^b \frac{df}{dx}(x') dx' \approx \frac{b-a}{N} \sum_{i=0}^{N-1} \frac{df}{dx}(x_i) .$$

The additional term for the second order approximation is $1/2(b-a)\delta f''$. Second, the derivative is approximated by

$$\frac{df}{dx} \approx \frac{f(x+s) - f(x)}{s} .$$

The next term in the Taylor expansion is $-1/2(b-a)s f''$. The total error of Eq. 3.4 is of the order

$$\delta s = \frac{1}{2} c_c (\delta s - s^2) f'' = \frac{1}{2} c_c s (\delta - s) f'' . \quad (3.5)$$

The ideal case for the averaging procedure is given by equally spaced measurements. In addition the spacing of the measurements s is the same as the signal s . This case can easily be verified, since in the sum

$$\sum_{i=0}^{N-1} f(x_i + s) - f(x_i)$$

all terms except the first and the last cancel. Thus, the sum is equal to $f(b) - f(a)$. The errors of the two approximations cancel each other and the calculation of the signal following Eq. 3.4 is exact. In summary, for the ideal case, the cancellation can be shown without any assumption on the system's characteristic curve $f(x)$. Furthermore, no approximation has to be made for this case.

In a nonideal case, for which some measurements are missing or the distance between two measurements x_i and x_{i+1} differs, the above approximations have to be used. More information on this subject can be found in uncertainty analysis of the nonlinearity (section 7).

The method is relatively simple as far as the theoretical concept is concerned. The practical implementation of this averaging method is not always so easy. In case of a balance, the measurement of the signal s at different values x_i can be achieved by putting additional masses on the balance's pan.

THE CALIBRATION DEVICE

The calibration device was the practical implementation of the idea, outlined above. Two tasks were fulfilled by this device. First, the calibration was determined and second, different loads were put on the balance.

As indicated above, the uncertainty of the averaging procedure is proportional to $\delta - s$. Obviously, the step-size δ should be close to the signal s in order to minimize this error. The signal amplitude in our case was $\simeq 784 \mu\text{g}$. By choosing δ to be the same and assuming a uniform distribution of measuring points, 255 different positions x_i within the calibration range of 200 mg were necessary.

By using two sets of weights, each consisting of 16 masses, 256 steps could be implemented. The mass of a wire in the first set was $784\ \mu\text{g}$ and in the second set it was $16 \times 784\ \mu\text{g} = 12.5\ \text{mg}$. These masses were labeled auxiliary masses (AM). The masses in the first set were abbreviated by AM-1.1 to AM-1.16; those in the second set by AM-2.1 to AM-2.16.

With the 32 wires from both sets, measurements with 256 different loads were possible. To make things easier to explain, the term, load-step, is introduced. The load on the balance from now on is written in load steps. This integer number is equivalent to the number of small weights required to reach a certain load. The practical implementation of the load step was made as a matter of course by putting masses from AM-1 and AM-2 on the balance. Load step 0 corresponds to zero additional load on the balance. Load step 255 ($255 \times 784\ \mu\text{g} = 199\,920\ \mu\text{g}$) is realized by putting 15 wires of AM-1 and 15 wires of AM-2 on the balance. For example load step 53 is realized by putting 3 large and 5 small weights on the balance. Of course, the order of the masses was fixed by the arrangement of the handler. Thus the bias for the load step 53 consists of following masses: AM-2.1+AM-2.2+AM-2.3+AM-1.1+AM-1.2+AM-1.3+AM-1.4+AM-1.5. Basically 15 AM's in each set would have been sufficient; but by using 16, the setup was more symmetrical and some additional consistency checks were possible.

The auxiliary masses were made of stainless steel wires. The wire for the AM-1 set had a diameter of 0.1 mm; for the AM-2 set the diameter was 0.3 mm. The wires were cut and bent in the machine shop of the Physics Institute of the University Zürich. The fine trimming was done at the *Mettler-Toledo* mass production laboratory. HANS KÜNG and later HOLGER HAUSMANN allowed me to work in that laboratory. The fine trimming of the wire weights was done by an electro-chemical etching process. It should be noted, that the smallest commercial available weight (1 mg) is 30% larger than the weights of AM-1. Thus, the fine trimming was not easy and the desired value was missed by as much as $1\ \mu\text{g}$. In Table 3.11 the masses of the 16 AM's of both sets as used for the copper measurements are listed. The standard deviation was $1.5\ \mu\text{g}$ for set AM-1 and $2.3\ \mu\text{g}$ for set AM-2. The

mean value of the mass for AM-2 ($12\,533.1\ \mu\text{g}$) was $3.5\ \mu\text{g}$ greater than the desired value ($16 \times 783.1\ \mu\text{g} = 12\,529.6\ \mu\text{g}$). The steps were equally spaced with a standard deviation of $1.7\ \mu\text{g}$. The implementation of load step 255 gives a total bias of $199\,743.3\ \mu\text{g}$ on the balance. This is approximately one load step ($790\ \mu\text{g}$) less than the sum of the calibration weights. The wire weights were placed on and removed from the calibration device several times. Although a special tool was built to perform this task, several weights were lost. They were replaced by spare weights. Thus, the weights used, and consequently the standard deviations, varied slightly from measurement to measurement. Fig. 3.14 shows a picture of two AM's. In summary the auxiliary weights were made such that measurements in equal size steps over the whole calibration range were possible and the deviation from the ideal step size was less than 1 %.

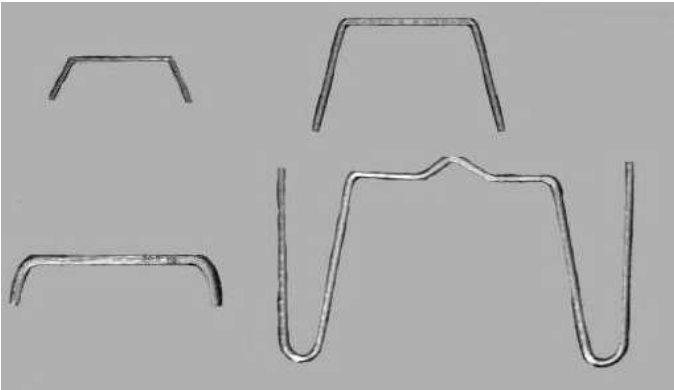


FIGURE 3.14: A picture of the used wire weights. The upper wires are type AM-1 and AM-2. The lower are the CM-2 (left) and CM-14 wires.

The calibration device, an apparatus to calibrate the balance and to implement the 256 load steps, was designed by *metrotec* and constructed in the physics-institute machine shop. The company *metrotec* had the experience in handling small weights. The important part of the handler is shown in Fig. 3.15.

i	mass of AM-1-i (μg)	mass of AM-2-i (μg)
1	783.0	12 530.8
2	781.8	12 530.7
3	782.6	12 530.4
4	784.0	12 533.4
5	783.7	12 534.0
6	781.7	12 531.8
7	783.3	12 537.4
8	782.8	12 535.5
9	786.4	12 531.8
10	783.6	12 535.1
11	781.0	12 531.6
12	785.2	12 535.5
13	781.5	12 531.3
14	781.5	12 535.9
15	784.3	12 531.7
16	780.2	12 528.0
mean (1-15)	783.1	12 533.1
std.dev. (1-15)	1.5	2.3

TABLE 3.11: Masses of the AM's. The mean and the standard deviation is calculated only from the first 15 weights.

The setup is symmetrical for the two wire sets. The wires rest on two parallel double-stairs with small circular grooves. For each mm downward movement of the double-stairs, a different wire is placed on a rod connected to the balance pan. The wires were placed symmetrically on the rod, to keep the center of mass close to the midpoint. By moving the double-stairs in the upward direction, one wire after another was removed from the balance. After the last wire was collected, one calibration weight was put on the balance. This was accomplished by a turn-around lever mounted at the top of the device. Thus, with two step motors the calibration and 256 load steps were implemented. The step

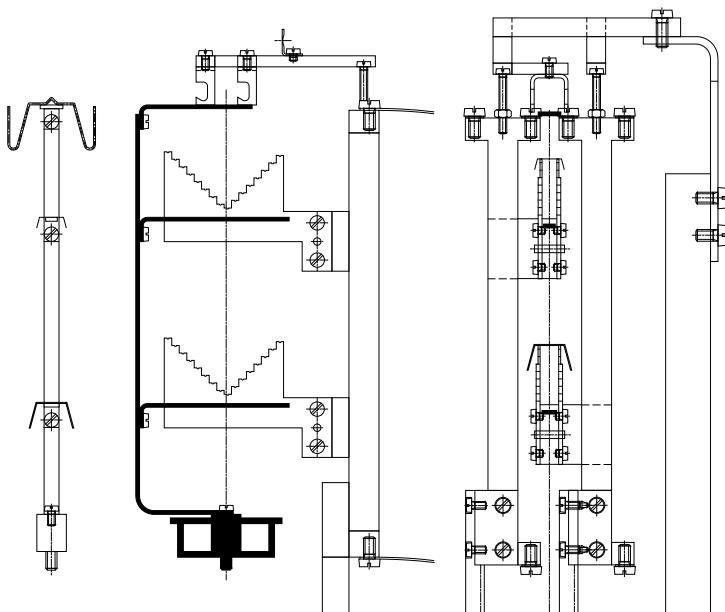


FIGURE 3.15: A technical drawing of the important part of the calibration device. The black parts were mounted on the pan of the balance. On the left, The CM-14, one piece of AM-1 and AM-2 put on the balance.

motors were mounted outside the vacuum tube in a Mu-Metal case. The movement was transferred into the vacuum tube by two rotary feed-throughs. The whole device was made of brass, copper aluminum and employed ceramics bearings to avoid changing the magnetic field.

Several parts had to be improved compared with the first version of the handler. Because of the very small mass of the weights in set AM-1, the adhesion forces were larger than the gravitational force. Sticking occurred when the handler was supposed to put the masses on the balance pan. Figure 3.16 shows

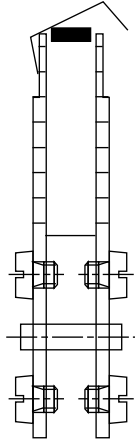


FIGURE 3.16: Sticking of a small wire on the double-stair.

the first phase of the sticking. The wire touches simultaneously the handler and the balance. In this phase the reading of the balance is distorted. By moving the double-stairs further down, the sticking breaks and the weight bounces on the rod and occasionally drop off. To overcome this problem several things were changed. The handler was coated with tungsten carbide to lower the sticking coefficient and the friction. In addition, the geometric dimensions were changed in order to lower the torque on the small mass produced by the sticking. Furthermore, the double-stair of the handler was ground by hand under a microscope. Each groove took the form of a small saddle. Fig. 3.17 shows the calibration handler mounted in the system.

Nevertheless, the handler was not perfect. After some time in vacuum, one or two and sometimes a few of the small wires caused problems due to sticking and fell off. One missing wire of AM-1 led to 16 missing load steps in the whole range. Fortunately, the missing steps were not consecutive, but uniformly distributed over the calibration range.

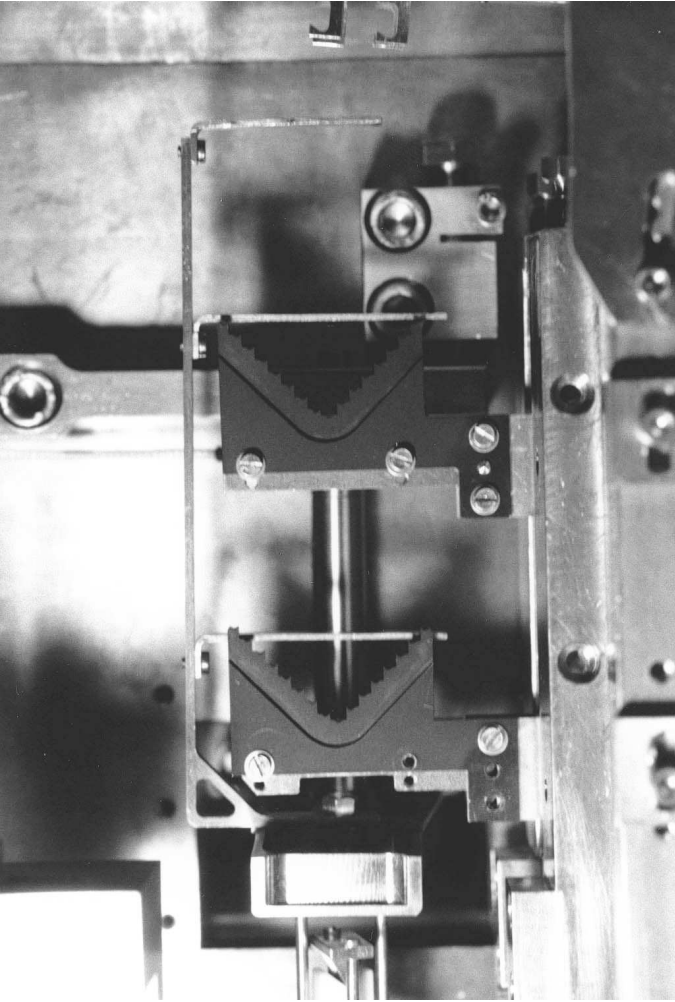


FIGURE 3.17: A picture of the calibration device during alignment work.

3.4.3 *The mass exchanger*

The TM's were alternately connected to the balance with the mass exchanger. During the exchange, the load on the balance was kept approximately constant.

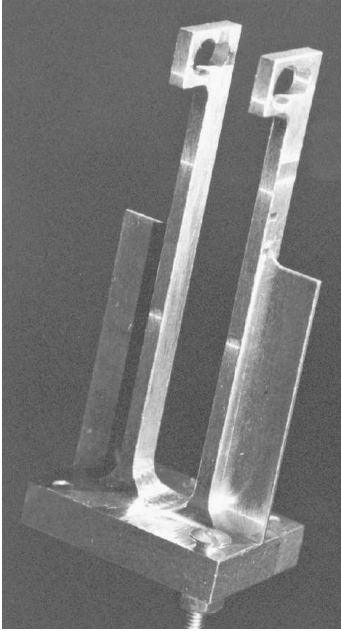
Each TM was either suspended on the balance or on a special lever arm. The lever arm (see Fig. 3.18) was basically a flat spring. It was designed using the finite elements methods(FEM) in such a way that it bent 0.6 mm with a load of 1.1 kg. By slowly moving the arm with a hydraulic system driven by a step motor, the load could be smoothly transfered onto the balance.

The mass transfer was done in such a way that one lever arms moved upwards to collect slowly the mass suspended on the balance. The other lever moved downwards in order to put the other mass on the balance. The balance output was monitored by the computer. The voltage across a piezo-electric element mounted above the balance pan was computer controlled, to keep the reading of the balance constant. The time needed for one mass exchange was typically 3 minutes. The variation on the balance reading was less than 100 mg. See Fig. 3.19 for a typical example of a mass exchange. A picture of the total mass suspension and parts of the mass exchanger can be seen in Fig. 3.18.

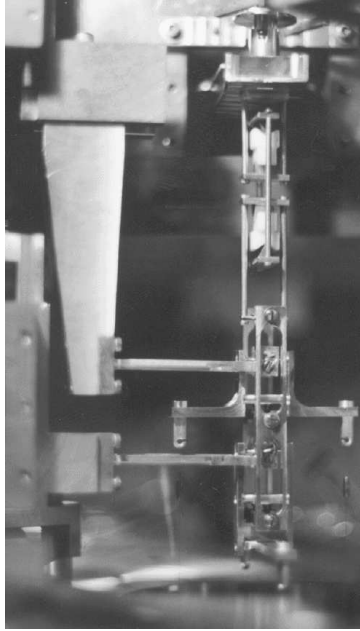
The original mass suspension has been described in detail in [17]. The most critical part of the suspension, the kinematic coupling has been improved in that it was remade of titanium and coated with tungsten-carbide (WC). This ensured the electrical grounding of the TM's during the weighing process.

3.5 CONTROLLING THE EXPERIMENT

In order to avoid disturbances due to human activity at the experimental site, the experiment was remotely controlled. Two computers were used. Both were connected to the internet so that one could login from the university. One computer controlled the measurement of the ambient parameters such as air pressure, humidity and several temperatures. In addition it was possible to set different temperatures with this computer. The second computer was used to read the balance and to drive the



(a) The elastic arm of the mass exchanger.



(b) The suspension of the test masses

FIGURE 3.18: Two pictures of the mass suspension. The left picture shows the lever arm and the right picture shows the whole mass suspension and parts of the exchange mechanism.

step motors for the mass exchanger and the calibration device. In addition, this computer controlled the field-mass drive. To ensure a precise timing for this computer a real time operating system was required. The operating system was Real-Time-Linux. Every night the measured data were automatically transferred to a computer located at the university.

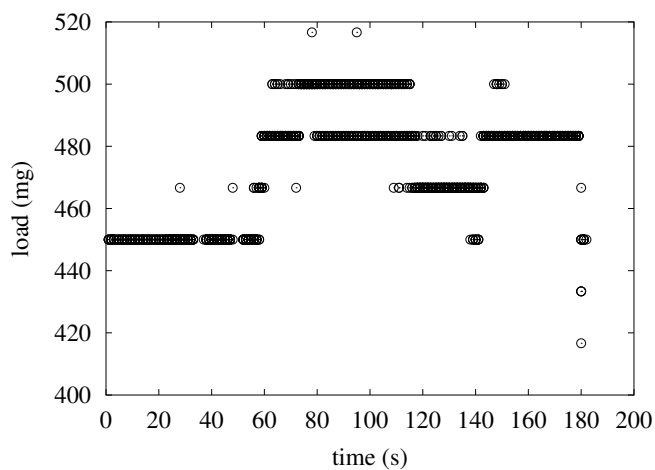


FIGURE 3.19: The reading of the balance measured during a typical mass exchange.

CHAPTER 4

DESCRIPTION OF THE MEASUREMENT PROCEDURE

In this chapter an overview of the measurement procedure and the online data analysis is given. The amplitude of the signal is measured for 256 load steps on the balance. To accomplish this, a few steps were needed. The smallest unit was the weighing of one TM. This was repeated four times with different load steps before the other TM was suspended from the balance. The weight difference (signal) was determined for eight different sets of four ($= 32$) load steps before the FM's were moved. The signal amplitude was determined for eight sets of 32 ($= 256$) load steps. This formed a complete measurement cycle. Before going into detail of the measurement procedure, some remarks on auxiliary measurements are given. The results of these auxiliary measurements were required in order to obtain an accurate value for the single weighing of one test mass.

4.1 AUXILIARY MEASUREMENTS TO CHARACTERIZE THE SYSTEM

Since the test masses were suspended on two tungsten wires, the whole system forms a pendulum. The pendulum motion of the test mass was almost never damped out. The quality factor of the pendulum was estimated to be 10^5 . The typical damping time was approximately half a week. The pendulum motion was excited almost all the time. First, seismic noise and human activities influenced the pendulum. Second, the influence of the mass

exchange on the test mass motion caused either an increase or decrease of the amplitude depending on the phase of the perturbation relative to the existing amplitude.

The pendulum motion was measured at the balance output. Two oscillation frequencies were observed in the balance output. One had the same frequency as the pendulum ν ; the other twice the frequency of the pendulum 2ν . To determine this frequency, one test mass was suspended from the balance for several days and the readings of the data were recorded. A Fourier transformation gave the frequencies of the pendulum motion (see Fig. 4.1).

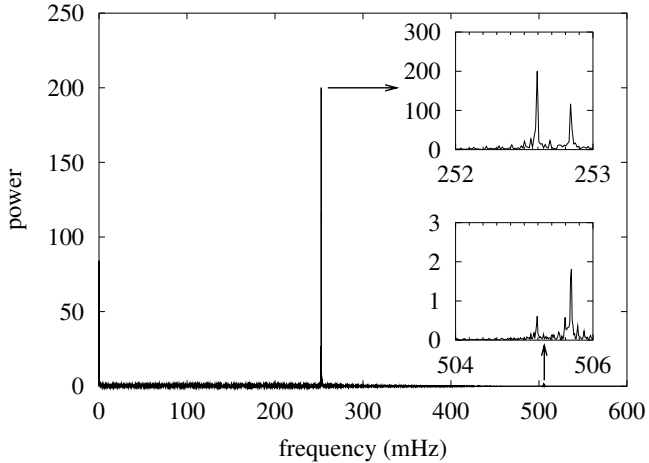


FIGURE 4.1: Data were taken for one day with the lower Ta-TM suspended on the balance. The Fourier transformed data are shown in this plot. The reason for the four peaks are explained in the text.

The oscillation with the frequency ν can be explained by side forces. The frequency 2ν is due to radial acceleration. First, some facts about the oscillation with frequency ν are presented. Although the balance measures primarily forces in the vertical direction, it has also a sensitivity to forces acting horizontally on the pan. Obviously, the sensitivity was much less for horizontal forces. Nevertheless, the side forces were appreciable. For ex-

ample, the length of the pendulum of the upper test mass was 2.5 m. Considering a pendulum amplitude of 0.25 mm, leads to a horizontal force equivalent to 110 mg.

Besides the oscillation amplitude of the test mass, there were a few additional factors which influenced the amplitude at the balance's output. The oscillation signal can be suppressed by choosing different filter settings. For instance when using MI 3, no oscillation could be seen. Of course, this is not the right way to solve the problem because the information of the oscillation amplitude and phase can be useful. By applying a fit technique to the readings, the determination of these parameters is possible. The influence on the signal amplitude of the other parameters can be studied. Consequently, the filter setting of the balance with the shortest time constant was used.

Interestingly, it was possible to change the sensitivity of the balance to horizontal forces. This was accomplished by changing the tilt of the balance. In [30] it is shown that a balance is sensitive to horizontal forces only when the beam is not precisely horizontal. In this balance, the position of the beam is measured by an optical system with respect to the balance's frame. The feed-back mechanism forces the beam to return to the position given by the optical system. Obviously, a tilt of the entire balance will also tilt the beam. The balance was leveled by watching the pendulum motion of the balance output. Nevertheless, the alignment procedure was not easy, and it was not possible to get rid of this oscillation completely. The tilt of the balance drifted slowly with time. Consequently, there was a small but continuous change of the horizontal sensitivity.

To make things more complicated, the amplitude of the pendulum motion changed periodically in time even under constant conditions. Figure 4.2 shows the reading of the balance for one tenth of a day. The observed behavior is a beat of two very close frequencies. The period of the beat is ≈ 1 hours for the upper and ≈ 2 hour for the lower TM. The mass suspensions allows the test mass to oscillate in two orthogonal directions. One direction was almost perpendicular to the beam of the balance. Thus, the balance was only slightly sensitive to that oscillation. Furthermore, the pendulum lengths for the two oscillations differed by

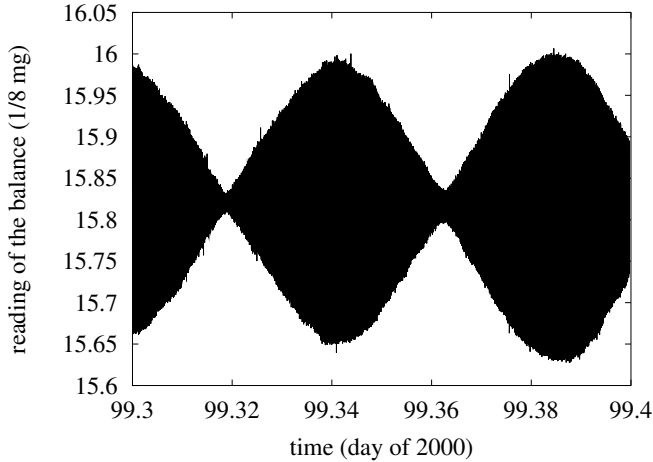


FIGURE 4.2: The reading of the balance vs. time for the lower mass. The individual period (≈ 4 s) of oscillation can not be seen here. Only the change of the amplitude of the oscillation is visible.

8 mm. Consequently the frequencies differed slightly resulting in a modulation of the signal with the difference frequency. The frequencies (ν_1, ν_2) were determined using a Fourier transformation. In Table 4.1 an overview is given. These frequencies can be used to determine precisely the length of each pendulum. Apart from the modulation phenomena, it was sufficient for most purposes to use only the two average frequencies $\nu = (\nu_1 + \nu_2)/2$ and $2\nu = (2\nu_1 + 2\nu_2)/2$.

The occurrence of the oscillation of the balance output with the same frequency as the test mass pendulum (ν) is explained above. The explanation for the oscillation with the frequency 2ν is the acceleration force of the pendulum's motion. Every time, the pendulum swings underneath the suspension point (twice per period) a maximum in the centrifugal force occurs. Again, two slightly different frequencies were observed for each test mass. Both frequencies were exactly the double of ν_1 and ν_2 . The amplitudes of these oscillations with frequencies $2\nu_1$ and $2\nu_2$ were

		Cu-TM		Ta-TM	
		upper	lower	upper	lower
ν_1	(mHz)	317.929	253.195	318.482	252.839
ν_2	(mHz)	317.406	252.931	317.991	252.592
$\Delta\nu$	(mHz)	0.523	0.253	0.491	0.247
l_1	(mm)	2 457.69	3 875.04	2 449.16	3 885.96
l_1	(mm)	2 465.79	3 883.14	2 456.74	3 893.57
Δl	(mm)	8.10	8.10	7.58	7.61

TABLE 4.1: The measured oscillations frequencies. The length were calculated using the equation of the mathematical pendulum. For the local acceleration the value $g = 9.807\,233\,5\,ms^{-2}$ was used.

much less than those of the lower frequencies (see Fig. 4.1).

To understand this, two aspects should be considered. First, the maximum of the centrifugal force of a pendulum is $F_{max} = A^2/l^2gm$. Assuming a pendulum amplitude of $A = 0.25\,mm$, the maximum force is $11\,\mu g$. A comparison with the side forces, which can be calculated with A/lgm ($110\,mg$), shows clearly that the centrifugal forces were smaller by several orders of magnitude.

Furthermore, the low pass characteristic of the balance has to be taken into account. The frequency ν was above the cutoff of the low pass filter. As shown in section 3.4.1 the filter characteristic of the balance showed a steep ν^{-8} behavior. Thus, the transfer of the higher frequency 2ν was approximately $256 = 2^8$ less than that of the lower frequency ν .

4.2 WEIGHING ONE TEST MASS

The result of the weighing of one test mass is basically one number, the weight of one test mass. The signal due to the oscillations, mentioned in the previous section was removed by making a least squares fit. The detailed fitting procedure is explained in this section.

First, the FM's were moved to position T and the lower test mass was suspended by means of the mass exchanger on the bal-

ance. After the last motor had stopped, the computer waited 40 s before readings from the balance were taken. This time was important in order to ensure that the measurements were not correlated with the previous measurements and to the changes of load, field mass, etc. After this pause, the measurements from the balance were stored in the computer. In total, 103 readings were taken in 39 s. In order to have the possibility of repeating disturbed measurements, an online data analysis was performed. The data were described by

$$y(t) = O + B_1 \sin(2\pi\nu t) + B_2 \cos(2\pi\nu t) + B_3 \sin(2\pi 2\nu t) + B_4 \cos(2\pi 2\nu t) . \quad (4.1)$$

A least squares fit was made in order to obtain best values of the parameters O , B_1 , B_2 , B_3 and B_4 . Eq. 4.1 is equivalent to the somewhat more easily understood form

$$y(t) = O + A_1 \sin(2\pi\nu t + \phi_1) + A_2 \sin(2\pi 2\nu t + \phi_2) \quad (4.2)$$

with $A_{1,2} = \sqrt{B_{1,3}^2 + B_{2,4}^2}$ and $\phi_{1,2} = \arctan(B_{2,4}/B_{1,3})$.

In the Eq. 4.1 the dependence on all of the unknown parameters is linear. Thus, it was more suitable for an online data analysis because a linear fit can be solved without iteration. A typical example of data and the fitted function is shown in Fig. 4.3. For the function shown, the amplitude for the lower frequency was $3 \mu\text{g}$ and $0.019 \mu\text{g}$ for the double frequency. The calculated χ^2 was $8.9 \mu\text{g}^2$. The number of degrees of freedom for fit was $\nu = 103 - 5 = 98$. For uncorrelated data points, one would estimate from the value of χ^2 that the noise for a single point was $0.301 \mu\text{g}$. Although this estimate is not completely valid (the data are correlated), it gives an order of magnitude for the noise of the balance.

The weighing of the test mass ended by storing the six parameters and χ^2 in the computer. The mean value O represents the weight of the test mass. Only this number was used for the calculation of the gravitational constant. For diagnostic purposes the amplitudes and phases, as well as the χ^2 of the fit were also stored. The amplitudes were used to show, that there were no

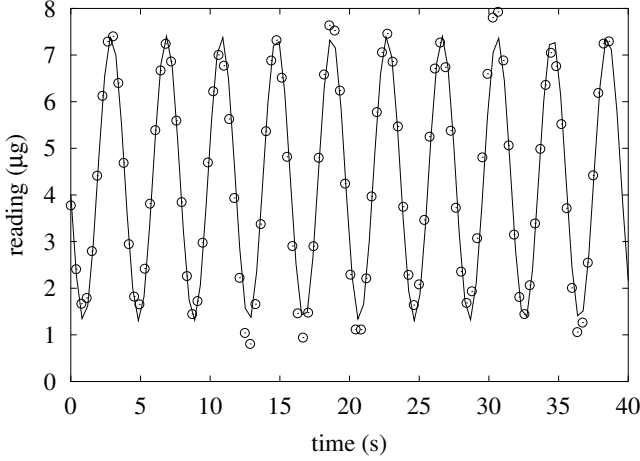


FIGURE 4.3: Measurement of the lower test mass. In 39 s total 103 readings from the balance were taken. The function, explained in the text, was fitted to the data points. For clarity, offsets have been removed from both axes and the vertical axis was plotted in calibrated units.

dependence of the measured values on the amplitudes of the oscillation. In addition, it could be shown, that the distribution of the amplitudes was the same for both field mass positions. Thus, even if there were a small error due to the pendulum oscillation, it would average to zero. For an undistorted pendulum, the phase varies slowly with time. Without going into detail, the reason for this can be found in the modulated signal and the fitting of only approximate oscillation frequencies. Some deviations from this behavior can be found among the data. Occasional deviations from this behavior occurred due to distant earthquakes and perturbations due to the nearby machine shop distorted the phase.

By analyzing the data online, perturbed measurements could be repeated. The criterium for repetition was a χ^2 greater than $28.7 \mu\text{g}^2$. The maximum number of repetitions was three. After that the measurement was stored and marked bad. Two main

reasons for such disturbances occurred. First, a large external excitation of the pendulum and second, the perturbation due to changing a small mass (see Fig. 3.16). An example of such a case is shown in Fig. 4.4 for which χ^2 is $157 \mu\text{g}^2$.

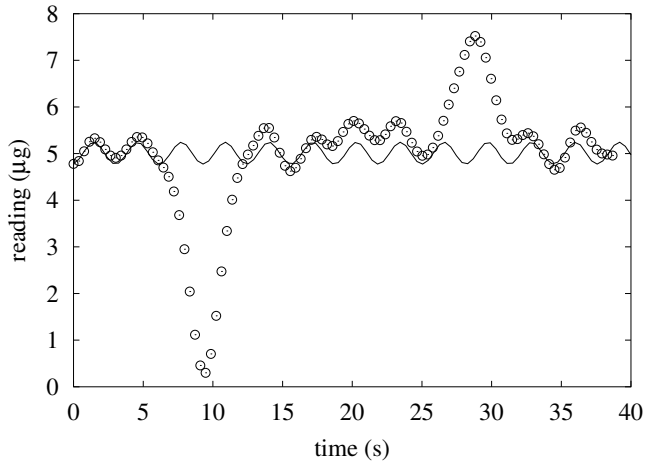


FIGURE 4.4: Measurement of the upper test mass. One of the auxiliary masses touched the balance and the calibration device. The χ^2 exceeded the designated limit for acceptance and the measurement was repeated.

4.3 ONE TEST MASS WITH DIFFERENT LOADINGS

The smallest unit of the measurement procedure was the weight determination of one test mass. This measurement was repeated four times with different loadings. For example, the mass of the lower test mass was determined with load step zero (no auxiliary masses on the balance's pan). Next, the weight was measured for the load steps one, two and three. The time to measure one test mass with four load steps, including the time for putting the weights on the balance, was typically 4.5 min.

4.4 THE WEIGHT DIFFERENCE

The next step involving the exchange of the TM's required to determine the weight difference was made. The lower TM was removed from the balance and the upper TM was connected to the balance. The weight was determined for the same four load steps. The masses were exchanged again and a measurement with the same four loadings was made. This cycle is shown in Fig. 4.5.

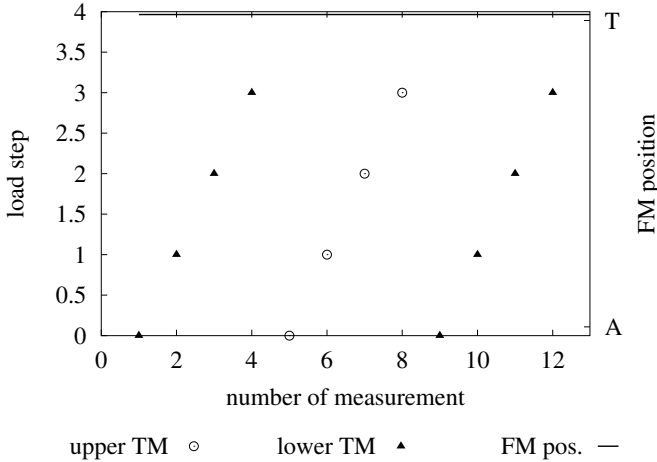


FIGURE 4.5: The weight difference determination for a LUL (lower, upper, lower test mass) cycle. Each test mass was measured with four load steps.

In mass metrology, making measurements A, B and A in order to compare the calibration mass A with the mass B is known as an ABA scheme. This means, measuring the known calibration mass, then the unknown sample and again the calibration mass. The advantage of this technique is that a linear drift of the balance is taken into account. In this experiment the same technique was used in various situations. To avoid confusion, this technique is labeled here LUL resp. ULU. The letters L and U are used to denote Lower test mass and Upper test mass. A complete

ULU cycle took 24 min.

4.5 WEIGHT DIFFERENCE FOR MORE LOADINGS

The measurement of the weight difference was the next step in the measurement procedure. Until now, a single LUL measurement with the load steps zero, one, two and three has been made.

The next measurement was a ULU measurement with the load steps four to seven. After this, a LUL measurement with the load steps eight to eleven was made. This scheme was repeated until the measurement with the load step 31 was completed. In all, eight ULU or LUL measurements were performed. In total, this gave 96 weighings. An overview of these measurements is shown in Fig. 4.6.

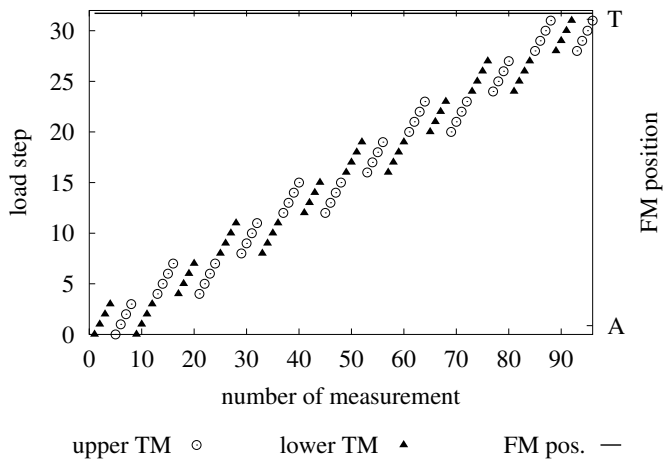


FIGURE 4.6: Eight ULU or LUL measurements.

4.6 THE SIGNAL AMPLITUDE

Until now, the field masses were in position T (together). The signal (test mass difference) in position T was measured for the load steps zero to 31. The field masses are moved to position A. The signal is measured for the load steps zero to 31. Finally, the FM's are moved to position T and the first measurement is repeated. Again an ABA-like measurement was performed. The abbreviation TAT (Together, Apart, Together) was employed to distinguish it from the ULU measurement. Over all, it took 12.5 hours to measure the 288 weighings of a complete TAT measurement. The scheme of such a measurement is shown in Fig. 4.7.

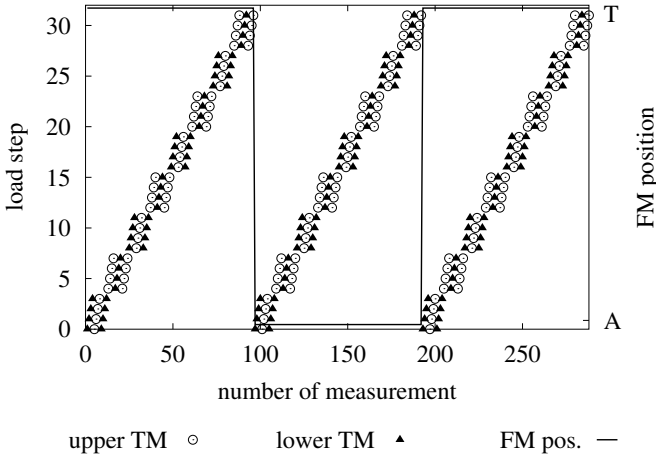


FIGURE 4.7: A complete TAT measurement.

4.7 CALIBRATION

After the measurement of the signal amplitude following an ATA or TAT scheme, the balance was calibrated. The calibration was carried out in such a way that the mean load on the balance

was 100 mg in order to minimize the self-heating of the balance. The calibration coefficient c_c was determined and both calibration weights were compared with each other. The calibration was carried out in the following manner:

First, CM-14 then CM-2 and finally CM-14 were put on the balance. From this ABA measurement the mass difference could be obtained. Next, the measurement of the empty balance was made; then both CM's were measured; again the empty balance and finally both CM's were measured. From this ABAB cycle the calibration coefficient could be determined.

For the measurements explained above, seven weighings were made. As shown in Fig. 4.8, the calibration was made alternately with the upper and lower mass suspended from the balance. As discussed in section 3.4.1, the calibration caused a small heating of the balance. To minimize the influence of the heating on the next measurements, nine measurement of upper and lower test mass were performed without using them in the data analysis. During these dummy weighings, the load step on the balance was chosen to be close to that of the next measurements.

4.8 THE SIGNAL AMPLITUDE FOR MORE LOAD STEPS

Up to this point, the signal amplitude for the first 32 load steps was measured. In all, eight such ATA or TAT measurements were needed to measure the signal amplitude at 256 load steps (from 0 to 255). The eight ATA/TAT measurements were named a measurement cycle. For a complete measurement cycle, 2416 measurements were needed (see Fig. 4.8). It took approximately 4.5 days to complete one cycle. In the cycle explained here, the loading on the balance was continuously increased. In the next cycle, the load was decreased.

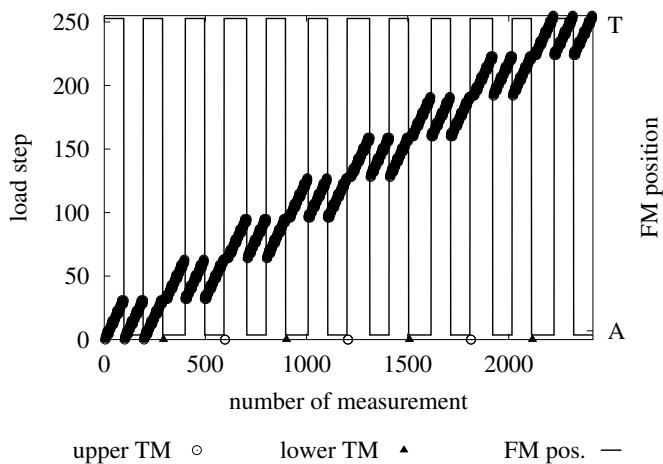


FIGURE 4.8: A complete measurement cycle. The occasional points at zero load represent the calibration measurements and are not shown in detail.

CHAPTER 5

DATA AND THEIR ANALYSIS

In this chapter some measured data are shown and some remarks on the data analysis are given. The structure of this chapter is similar to chapter 4. It starts with the calculation of the weight difference (signal) and continues with the calculation of the amplitude of the signal. In the next section, the calibration data will be discussed. Finally a summary of all data is given

5.1 CALCULATION OF THE SIGNAL

The raw data for one measurement cycle is shown in Fig. 5.1. In a first step, the data related to the balance calibration and the dummy measurements were removed from the analysis. From the remaining data, the signal, defined as the weight difference of upper and lower test mass was computed. As described in 4.4 three measurements (ULU) were made. All ABA-measurements were analyzed the same way. In the following equation y_{A1} , y_B and y_{A2} denote the value of the measurements whereas t_{A1} , t_B and t_{A2} stand for the times when the measurements were taken. The ABA-difference was calculated using

$$d = y_B - \left(y_{A1} + \frac{y_{A2} - y_{A1}}{t_{A2} - t_{A1}} (t_B - t_{A1}) \right), \quad (5.1)$$

which is based on a linear time dependence of the drift. The expression in the parentheses gives a linear estimate of the value of the A measurement at the time the B measurement was made.

The difference d is associated with the time t_B . This is important, if the difference is used for further data processing.

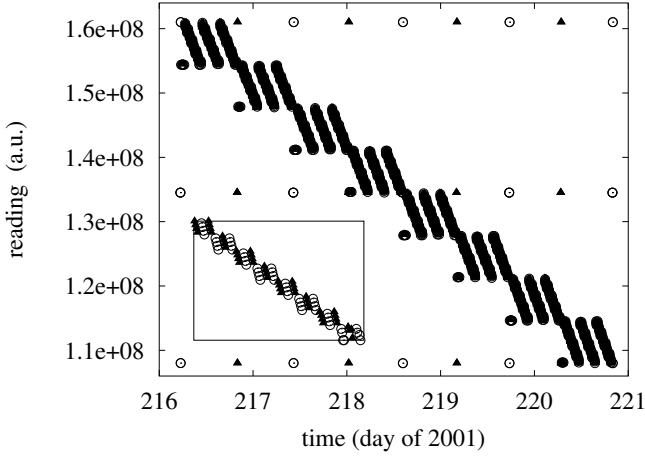


FIGURE 5.1: Measured weights for one measurement cycle. The measurements with the upper test mass connected to the balance were plotted as points. The solid triangles denote measurements with the lower TM. The inset is a magnification of the first eight ULU measurements. The measurements in the middle combined with measurements at the top and bottom of the vertical axis determine the calibration.

In case of the ULU measurement, the signal s is calculated using the above formula. For the LUL measurement the result was multiplied by -1 , such that the signal is given by the weight of the upper test mass minus the weight of the lower test mass. The signal for a complete measurement cycle is shown in Fig. 5.2. The noise of the individual measurements is clearly visible (approx. 200 ng).

The two dashed lines in this figure represents a linear fit to the data. The slope indicate a small linear drift. The reason for this drift is that the water surface on the test masses had not stabilized when this measurement was made. The drift during the first 10 days after evacuation of the vacuum system is of order

100 ng/day. After this time, the drift vanished. Nevertheless, the drift is very smooth and linear, such that any influence on the measurement of the difference was completely negligible. The loss of 100 ng water corresponds to a water film on one test mass of a thickness of 7.1 nm or approximately 24 monolayers.

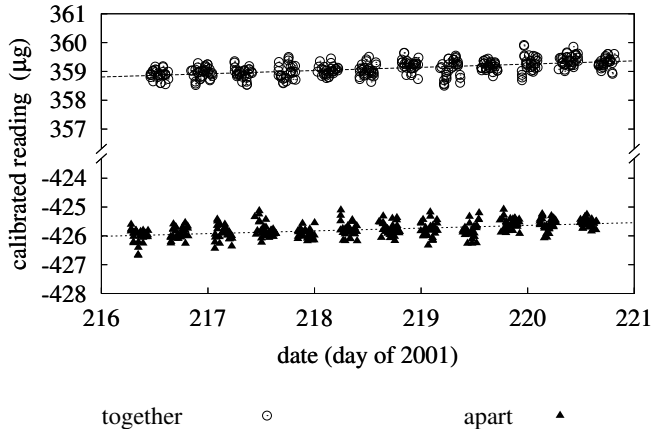


FIGURE 5.2: The signal extracted from the raw data shown in Fig. 5.1. The break in the vertical axis should be noticed. The dashed lines correspond to linear fits to the data in each field mass position.

5.2 THE AMPLITUDE OF THE SIGNAL

The signal was measured in both FM positions. As described in section 4.6, three measurements (TAT) were made. The difference of the signal in position apart and together was determined with Eq. 5.1. The signal amplitude was calculated for the 256 load steps. In Fig. 5.3 the signal amplitudes of this measurement cycle is shown versus load step.

Ideally, 256 signal amplitudes were obtained for one measurement cycles. As already discussed in section 3.4.2, some

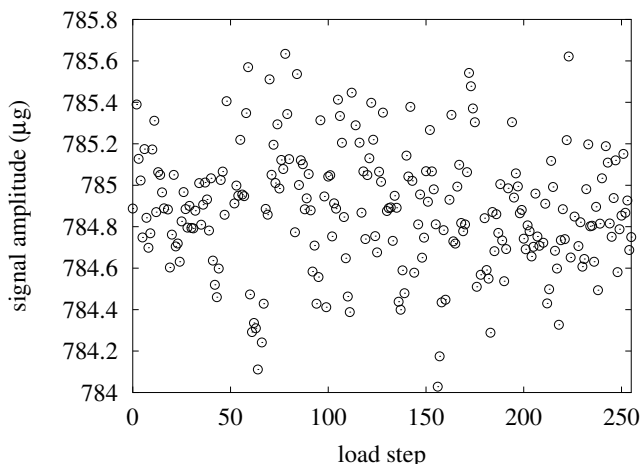


FIGURE 5.3: The signal amplitude versus load step.

AM's caused problems and the measurements failed. These measurements were already identified during the weighing process (see 4.2) and not included in the analysis. Thus, several steps are missing in the plot of Fig. 5.3.

Typically the signal amplitude was determined for approximately 220 different load steps. From this data a mean value and an error of the mean was calculated. This was done for each measurement cycle. This is the first point of the analysis in which a statistical uncertainty is introduced. As discussed in 4.2, it was not possible to deduce a statistical uncertainty for the weighing of the single test mass due to a numerical problem in determining the inverse covariance matrix. Thus, it was also not possible to calculate an uncertainty for the weight difference.

5.3 EVALUATION OF THE CALIBRATION DATA

The signal amplitude obtained for each measurement cycle was multiplied by a calibration coefficient. The calibration coefficient

was calculated from the ABAB measurement as described in section 4.7 (A= only one TM suspended to the balance, B= CM-2 and CM-14 additionally on the balance). By using the above difference method, the values for the ABA and for the BAB measurement were calculated. The mean value of both measurements were computed and used for the calibration. The difference was monitored. No unreasonably large differences were observed indicating the absence of systematic errors. The heating of the balance (see section 3.4.1) was different for ABA than BAB measurement. Therefore, a change in the balance's sensitivity due to the heating would affect both measurements differently. The relative difference in the calibration coefficient for both measurements was of the order of 10^{-7} . This was negligible compared with the typical uncertainty of the calibration (4 ppm).

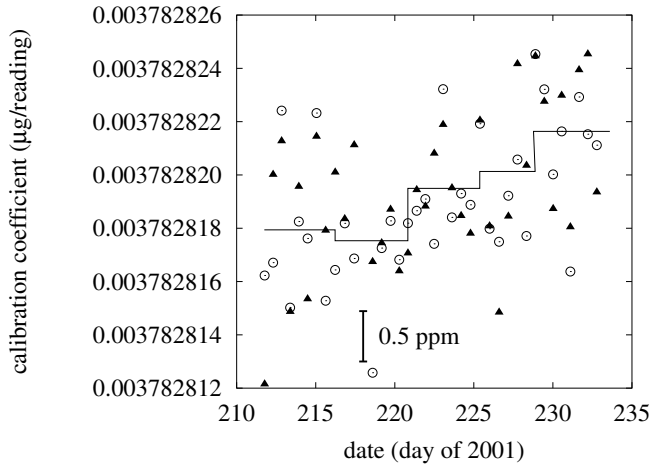


FIGURE 5.4: The calibration coefficient for 25 days of measurement (5 cycles). The open circles were measured by putting the calibration masses on the empty balance. In contrast, the solid triangles were measured by taking away the calibration masses. Both measurements agree within their uncertainty. The solid line gives the calibration values as used to calibrated the data of the individual cycles.

During a measurement cycle the calibration coefficient varies typically by 5×10^{-7} . Therefore, the average value was used to calibrate the complete measurement cycle. In Fig. 5.4, the calibration coefficient versus time is shown for five measurement cycles.

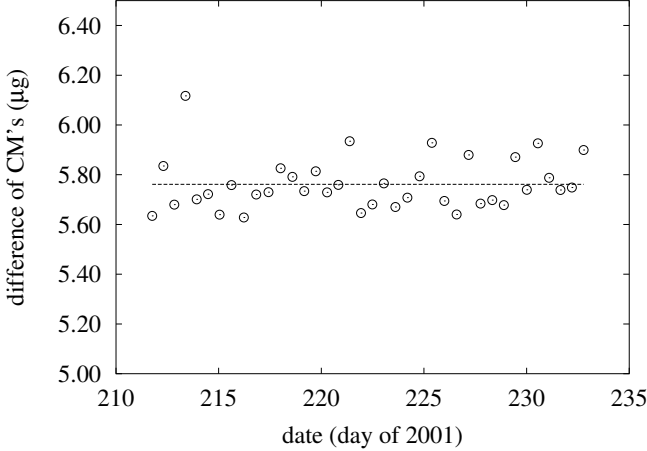


FIGURE 5.5: The measured difference between the calibration mass CM-14 and CM-2.

Besides the determination of the calibration coefficient, both CM's were compared with each other in the calibration process. The results of these comparisons for the same time period is shown in Figure 5.5. The values of the mass difference in this plot is already multiplied with the calibration coefficient. The scattering of the measurements is typically 100 ng. No linear drift was found in the difference data. The measured mass difference is compared with the mass difference determined at metas. This value was 6.4(8) ng. This is in good agreement within the measurement uncertainty of the experimental value (5.76(2) ng) obtained with the balance.

5.4 SUMMARY OF THE DATA

In all three measurement series were taken. One series was measured with copper TM's and two series with the tantalum TM's. The series were abbreviated by Cu, Ta-I and Ta-II. The two series measured with the tantalum TM's differ in the FM position. The field mass positions used in the Ta-II measurements were the same as those used in the Cu-series. In Table 5.1 an overview of all three measurements is given.

	Cu	Ta I	Ta II
begin of measurement	31.07.01	09.01.02	11.04.02
end of measurement	07.09.01	08.03.02	10.05.02
number of cycles	8	3 (130) ^a	6
signal amplitude (μg)	784.8615	789.6129	788.5834
statistical uncert. (ppm)	6.9	7.1	8.4

^aThe 130 cycles were measured with only 16 loadings.

TABLE 5.1: Overview of the three measurement series.

The first measurement series (Cu) was made between the 31st July 2001 and the 7th September 2001. In total 8 cycles were measured for this series. The calibrated amplitude of the signal for the eight measurement cycles is shown in Fig. 5.6. The statistical relative uncertainty for this measurement was 6.9 ppm. The calculation of the mean value leads to a $\chi^2_{Cu} = 7.7$ which is to be compared with seven degrees of freedom.

The second measurement series (Ta-I) was made between the 9th January 2002 and the 8th March 2002. Only three measurement cycles with 256 steps were completed before problems with the small weights occurred. Subsequently, only measurements with the AM-2-set were made. In total 130 of these cycles were measured. The statistical relative uncertainty of the data for the signal amplitude was 7.1 ppm. The signal amplitude is shown in Fig. 5.7. Only the first three data points of this plot were measurements of complete cycles with 230 load steps. The other measured points were averaged by measurements with only 16

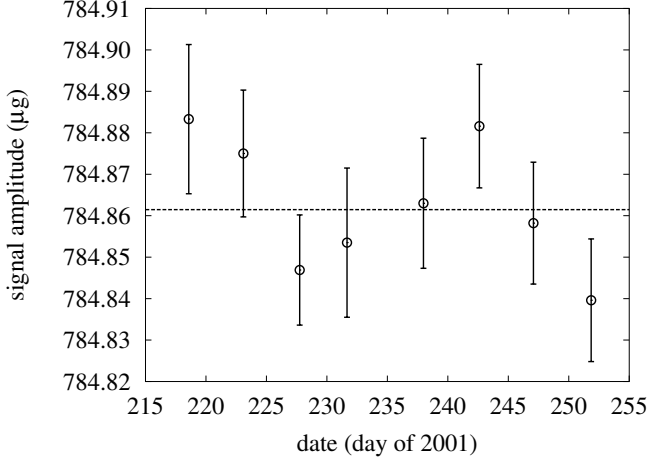


FIGURE 5.6: Results of the measurement series Cu. Only statistical uncertainties are shown.

load steps. The $\chi^2_{TaI} = 15.4$ for six degrees of freedom. The probability for this χ^2 is 2 %. Since, the last four points of Fig. 5.7 were made with only 16 load steps they could have had a larger systematic uncertainty than the first three points which were measured with 230 load steps. This could explain the high χ^2 .

The third measurement series (Ta-II) was measured between the 11th April 2002 and the 10th May 2002. In total 6 cycles were measured. As in the previous measurement, problems due to sticking of the small wires occurred. Until the end of the measured series, 8 of the original 16 small wires fell from the handler. The data measured in this configurations are plotted in Fig. 5.8. The statistical relative uncertainty of the signal amplitude was 8.4 ppm. For this measurement series one obtains a $\chi^2_{TaII} = 3.7$ for five degrees of freedom.

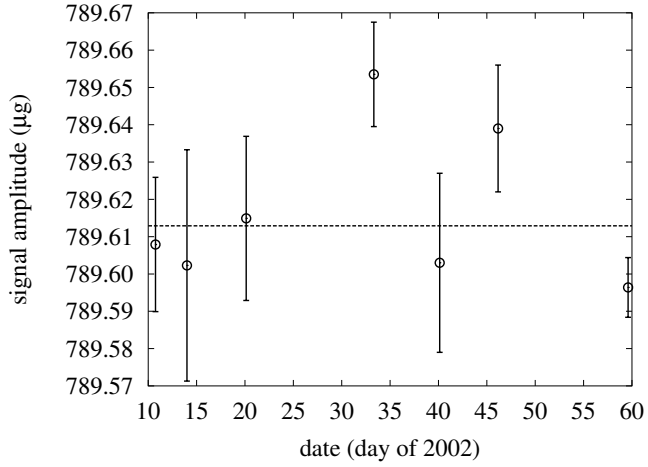


FIGURE 5.7: Results of the measurement series Ta I.

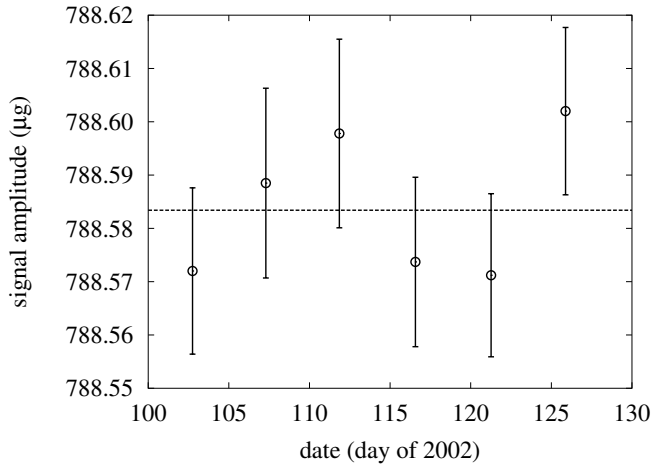


FIGURE 5.8: Results of the measurement series Ta II.

CHAPTER 6

PRACTICAL ASPECTS OF THE MASS INTEGRATION

In this chapter a brief introduction to the mass integration is given. The mass integration is a common feature of all experimental determinations of the gravitational constant. Basically, a force or a torque is measured experimentally, and a value for G is determined by comparing this value with the calculated force or torque. Each experiment has its particular symmetries such that the methods of mass integration differ appreciably.

The mass integration for this experiment was programmed principally by EUGEN HOLZSCHUH and WALTER KÜNDIG. They developed the main equations for the mass integration and the computer programs to calculate the gravitational force. The basic aspects of the mass integrations are reported in the next three sections. First, the basic equations are derived. Second, a technique, called "automatic differentiation" is introduced. This technique allows higher order derivatives to be calculated without determining analytically these derivatives. Nevertheless, this technique was superior with respect to roundoff errors to numerical differentiation. Third, some values of the mass integration are summarized.

6.1 BASIC EQUATIONS FOR THE MASS INTEGRATION

In this section, the basic equations for the mass integration are introduced. The two important parts, the calculation of the field for a given source mass and the calculation of the force on a test

mass in this field are presented. For simplicity, perfect cylindrical symmetry is initially assumed. The section ends with some remarks on other nonsymmetric parts of the mass distribution.

6.1.1 The field of a hollow-cylinder

The gravitational potential of a body (field mass) at a point \vec{r} is given by the equation

$$\Phi(\vec{r}) = \int \int \int \varrho_{FM} G \frac{1}{|\vec{r} - \vec{r}'|} dV'. \quad (6.1)$$

The density of the FM is given by ϱ_{FM} . In general the density is a function of the position \vec{r} . In the following, the density is assumed to be constant throughout the whole FM. In addition the FM is taken to be a hollow cylinder (inner radius R_1 , outer radius R_2 and height $2B$). The origin of the coordinate system is located at the geometrical center of the cylinder. Furthermore, only the potential along the z-axis is of interest. With these assumptions the potential on the axis can be calculated with the equation

$$\Phi(0, 0, z) = \varrho_{FM} G \int_0^{2\pi} d\phi \int_{-B}^B \int_{R_1}^{R_2} \frac{r' dr' dz'}{\sqrt{r'^2 + (z' - z)^2}}. \quad (6.2)$$

This three dimensional integral can be solved analytically. The solution is given by the equation

$$\begin{aligned} \Phi(r = 0, \phi = 0, z) = \varrho_{FM} G \pi \bigg[& (B - z) r_2^- + (B + z) r_2^+ \\ & + R_2^2 \ln \left\{ \frac{B - z + r_2^-}{-(B + z) + r_2^+} \right\} - (B - z) r_1^- \\ & - (B + z) r_1^+ - R_1^2 \ln \left\{ \frac{B - z + r_1^-}{-(B + z) + r_1^+} \right\} \bigg] \end{aligned} \quad (6.3)$$

with

$$r_{1,2}^\pm = \sqrt{R_{1,2}^2 + (z \pm B)^2}.$$

The gravitational field in z-direction is given by the first derivative of the potential. For the field of Eq. 6.3 this leads to the compact Eq. 2.1 or Eq. 6.15.

From the potential on the z-axis, the potential at points close to the axis can be calculated using the expansion

$$\Phi(r, \phi, z) = a_0 + a_1 r + a_2 r^2 + a_3 r^3 + \dots = \sum_{i=0}^{\infty} a_i r^i \quad (6.4)$$

with unknown coefficients a_1, a_2, \dots and $a_0 = \Phi(0, 0, z)$. The gravitational field satisfies the Laplace equation $\nabla^2 \Phi = 0$. Applying the Laplace operator in cylinder coordinates to Eq. 6.4 leads to

$$a_1 r^{-1} + \sum_{i=0}^{\infty} r^i \left(\frac{\partial^2 a_i}{\partial z^2} + (i+2)^2 a_{i+2} \right) = 0. \quad (6.5)$$

This equation is true independent of the value of r . For reasons of symmetry, the factor a_1 must equal zero and therefore every a_i with odd i equals zero as well. Thus, the values for a_i can be calculated recursively from

$$a_{i+2} = -\frac{1}{(i+2)^2} \frac{\partial^2 a_i}{\partial z^2} \quad (6.6)$$

with $a_0 = \Phi(0, 0, z)$. Using the abbreviation $V := \Phi(0, 0, z)$ and $V^{(n)}$ for the n th derivation of V with respect to (wrt) z , one obtains the first five coefficients, $a_0 = V$, $a_2 = -1/4 \partial^2 V / \partial z^2$, $a_4 = 1/64 V^{(4)}$, $a_6 = -1/2304 V^{(6)}$ and $a_8 = 1/147456 V^{(8)}$. By induction it is easily shown, that the coefficient a_{2n} is

$$a_{2n} = \left(-\frac{1}{4} \right)^n \frac{1}{(n!)^2} V^{(2n)}. \quad (6.7)$$

Using this expression for the coefficients in the expansion 6.4, the gravitational potential can be calculated from the sum

$$\Phi(r, \phi, z) = \sum_{i=0}^{\infty} \left(-\frac{1}{4} \right)^i \frac{1}{(i!)^2} V^{(2i)} r^{2i}. \quad (6.8)$$

Thus, the gravitational field in z-direction is given by

$$g_z(r, \phi, z) = \sum_{i=0}^{\infty} \left(-\frac{1}{4} \right)^i \frac{1}{(i!)^2} V^{(2i+1)} r^{2i}. \quad (6.9)$$

6.1.2 The force on a cylinder

The gravitational force on a cylindrical mass (density ϱ_{TM} , diameter $2r$ and height $2b$) can be calculated from the integral

$$F_z = \varrho_{TM} \int_0^{2\pi} d\phi' \int_{-b}^{+b} dz' \int_0^r g_z r' dr' . \quad (6.10)$$

In this section, the origin of the coordinate system is at the center of the cylinder. By using the Eq. 6.9 the force can be calculated from the sum

$$F_z = \varrho_{TM} 2\pi \sum_{i=0}^{\infty} \left(-\frac{1}{4}\right)^i \frac{1}{(i!)^2} \int_{-b}^{+b} dz' \int_0^r V^{(2i+1)} r'^{2i} r' dr' . \quad (6.11)$$

The integration over r is trivial. The integration over z is

$$\int_{-b}^{+b} V^{(2i+1)} dz' = V^{(2i)}(b) - V^{(2i)}(-b) .$$

Making a Taylor expansion for small b one obtains

$$\begin{aligned} \int_{-b}^{+b} V^{(2i+1)} dz' = & \\ & V^{(2i)}(0) + bV^{(2i+1)}(0) + \frac{1}{2!}b^2V^{(2i+2)}(0) + \dots \\ & -V^{(2i)}(0) + bV^{(2i+1)}(0) - \frac{1}{2!}b^2V^{(2i+2)}(0) + \dots \end{aligned}$$

Adding similar terms gives

$$\begin{aligned} \int_{-b}^{+b} V^{(2i+1)} dz' = & \\ & 2bV^{(2i+1)}(0) + \frac{2}{3!}b^3V^{(2i+3)}(0) + \frac{2}{5!}b^5V^{(2i+5)}(0) + \dots \end{aligned}$$

or

$$\int_{-b}^{+b} V^{(2i+1)} dz' = \sum_{j=0}^{\infty} \frac{2}{(2j+1)!} b^{2j+1} V^{(2i+2j+1)} . \quad (6.12)$$

The final equation for the gravitational force on a cylinder can be calculated by merging Eq. 6.8 and Eq. 6.12 to obtain

$$F_z = 2br^2\pi\varrho_{TM} \sum_{n=0}^{\infty} V^{(2n+1)} \sum_{i=0}^n \frac{1}{(-4)^i} \frac{1}{i! (i+1)!} \frac{1}{(2(n-i)+1)!} b^{2(n-i)} r^{2i} \quad (6.13)$$

The force on a cylindrical mass can be easily calculated with this equation. Only the odd derivatives of the potential at the center of the cylinder have to be known. An easy way to calculate these derivatives is described in section 6.2. The first terms are given by

$$\begin{aligned} \frac{F_z}{M_{TM}} &= \frac{\partial V}{\partial z} \\ &+ V^{(3)} \left(\frac{1}{6} b^2 - \frac{1}{8} r^2 \right) \\ &+ V^{(5)} \left(\frac{1}{120} b^4 - \frac{1}{48} r^2 b^2 + \frac{1}{192} r^4 \right) \\ &+ V^{(7)} \left(\frac{1}{5040} b^6 - \frac{1}{960} r^2 b^4 + \frac{1}{1152} r^4 b^2 - \frac{1}{9216} r^6 \right) \\ &+ \dots \end{aligned}$$

The convergence of this series in a volume larger than the volume of the test mass was proved by EUGEN HOLZSCHUH [31]. A faster convergence in the mass integration program was achieved by splitting the long cylinders, such as the main cylinder of the test mass, into two cylinders, each having the half height of the original cylinder. In Fig. 6.1 the first three terms of this series are shown. In this figure, the force on a single cylindrical body of the size of the copper and tantalum test mass due to the mercury cylinder is plotted as a function of the TM's position.

6.1.3 Integration of asymmetric parts

Both the TM's and the FM's were not completely symmetric. Besides the formula of the gravitational field of a hollow cylinder,

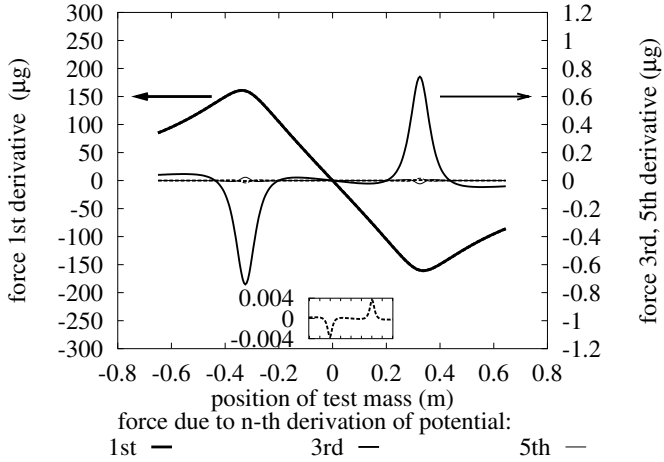


FIGURE 6.1: The force of one field mass on one test mass. The contributions of the first, third and fifth derivative of the potential are shown. The solid lines show the forces on the copper test mass; the dashed on the tantalum test mass. The small inset shows the gravitational force contributed by the third derivative of the potential for the tantalum test masses. This contribution is a factor of 200 smaller. The forces due to the first derivative is the same for both types of test masses.

EUGEN HOLZSCHUH implemented equations for the calculation of the fields of rotational bodies with triangular and circular cross sections. The field mass was divided into hollow cylinders (rotation body with rectangular cross section), O-rings, rings with triangular cross sections and point masses. The gravitational field of this objects were summed. Listed in Table 6.1 is the number of bodies of each type as related to one field mass.

The test masses were subdivided into smaller hollow cylinders and several point masses. Tests showed that the size of the subdivisions employed resulted in a relative error less than 0.5 ppm for both field and test mass.

rotation bodies with rectangular cross section	98
rotation bodies with circular cross section	4
rotation bodies with triangular cross section	91
point masses	338
sum	531

TABLE 6.1: Subdivision of one field mass.

6.2 INTRODUCTION TO AUTOMATIC DIFFERENTIATION

The mass integration was calculated with Eq. 6.13. Besides the different coefficients the derivatives of the potential have to be computed. The first derivative is given by

$$V^{(1)} = g_z(0, 0, z) = 2\pi\varrho G \left(r_2^+ - r_2^- + r_1^- - r_1^+ \right), \quad (6.14)$$

with $r_{1,2}^\pm = \sqrt{R_{1,2}^2 + (z \pm B)^2}$.

The higher derivatives have to be calculated starting with this equation. Thus, basically higher derivatives of the square root have to be calculated. Automatic differentiation provides a powerful method for evaluating higher order derivatives resulting in very small roundoff errors. Unfortunately, the method of automatic differentiation is largely unknown to physicists. Thus, a simple example of the method is given. In the following, f denotes the function $f = \sqrt{g}$ and g is a function, for which the n -th derivative exists. The first derivative of f is given by $f^{(1)} = g^{(1)}/(2f)$. From the last expression the product $ff^{(1)} = g^{(1)}/2$ can be calculated. The underlying rule for the automatic differentiation is the Leibniz's rule for the differentiation of a product which is

$$(fg)^{(n)} = \sum_{k=0}^n \binom{n}{k} f^{(k)} g^{(n-k)}. \quad (6.15)$$

Applying this rule to the product $ff^{(1)}$ gives

$$(ff^{(1)})^n = \frac{1}{2}g^{(n+1)} = \sum_{k=0}^n \binom{n}{k} f^{(k)} f^{(n+1-k)} .$$

This can be written as

$$\frac{1}{2}g^{(n+1)} = ff^{(n+1)} + \sum_{k=1}^n \binom{n}{k} f^{(k)} f^{(n+1-k)} .$$

After solving for $f^{(n+1)}$ and replacing the index $n+1$ by n , one obtains

$$f^{(n)} = \frac{1}{f} \left(\frac{1}{2}g^{(n)} - \sum_{k=1}^{n-1} \binom{n-1}{k} f^{(k)} f^{(n-k)} \right) . \quad (6.16)$$

With this equation the derivative of the order n can be calculated iteratively from the previous order and the derivatives of g . This equation is exact and in a computer implementation of this equation, roundoff errors are small.

According to Eq. 6.15 the function g is of the type $g = a + (z + b)^2$, with the constants a and b . For this function only the first three derivatives are nonzero. They can easily be calculated. In the mass integration software written by EUGEN HOLZSCHUH derivatives up to the 14th order were calculated and taken into account.

6.3 RESULTS OF THE MASS INTEGRATION

The mass integration was made for each individual measurement cycle. The value varied slightly from cycle to cycle due to small temperature and air pressure variation. The final analysis was made on the basis of their individual values. In Table 6.2 values of the signal amplitude as calculated for mean values of the mass integration is shown for the three measurement series. For these calculations the value $G = 6.67259 \times 10^{-11} \text{ m}^3 \text{ kg}^{-1} \text{ s}^{-2}$ was used. The variation from the mean was less than 1 ng (1.2 ppm). The reasons for the variation of the calculated signal were variations of the air density, the variation of the temperature of the

mercury and thus a variation of the mercury level in the compensation vessel. The effect of the displaced air on the total signal amplitude is of the order of 10^{-4} . Variation of the air density of the order of 10^{-2} changes the signal amplitude at the ppm level. Variations in the temperature of the mercury changes the mercury density slightly and therefore the mass distribution.

	Cu	Ta I	Ta II
calculated signal (μg)	784.703 7	789.435 3	788.405 2

TABLE 6.2: Results of the mass integration for the different setups used in the three measurement series. The given values are mean values.

6.4 UNCERTAINTY OF THE MASS INTEGRATION

The results, presented in the previous section, were calculated for an ideal mass setup. In reality, the mass setup varies slightly from the ideal setup. In addition, the uncertainty in the measurements have to be taken into account. Both facts are discussed briefly in this section.

First, deviation from the ideal concentric mass setup is considered. In this context ideal concentric means that the TM's were on the z-axis and were not tilted. The effect of tilted and off center TM's on the signal amplitude was investigated for both types of test masses. For the copper test mass, the results are shown in Fig. 6.2. These calculations were obtained by rotating the coordinate system of the test mass through a small angle relative to the coordinate system of the field mass.

Typically the dependence of the signal amplitude on eccentricity and tilt was very weak for small values. In the experiment the tilt was well below 1° and the distance between TM and z-axis was less than 0.5 mm. According to table 3.8, both copper test mass were almost 0.5 mm off center. Therefore an uncertainty of the mass integration of 4.7 ppm was taken into account. The tantalum test masses were much closer to the center. In addition, due to the smaller mass, the dependence on a tilt of

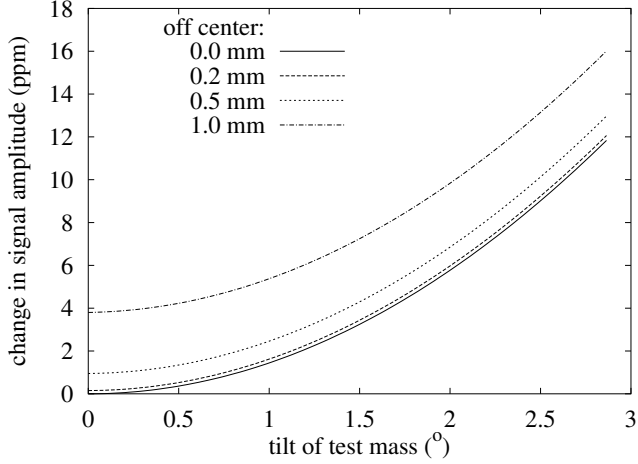


FIGURE 6.2: The calculated influence of tilt and off center parameters on the signal amplitude for the copper test mass.

the test mass was less. For measurements with the tantalum test mass, a relative uncertainty of 2.7 ppm was taken into account.

The numerical error of the mass integration was estimated by calculating the forces for a simplified ideal setup and comparing this value with the numerical calculation. This resulted in an uncertainty of 5 ppm.

The influence of the uncertainties in the knowledge of the exact distribution of the masses in the field and test masses was also investigated. This was investigated by varying several parameters determining the shape under the assumption of constant masses. This resulted in the uncertainty due to the TM mass distribution of 3.0 ppm for the copper test mass and 4.0 ppm for the tantalum test masses. The contribution due to the FM mass distribution was estimated to be 20.6 ppm. The contribution of the mass integration to the total uncertainty budget is listed in Table 6.3.

Finally, it should be noted that two programs for the mass integration were developed independently. Both were used for the estimation of the uncertainties. The results of the programs

source of uncertainty	contribution (ppm)		
	Cu	Ta I	Ta II
horizontal position of TM's	4.7	2.7	2.7
TM mass distribution	3.0	4.0	4.0
FM mass distribution	20.6	20.6	20.6
numerical integration	5.0	5.0	5.0

TABLE 6.3: The uncertainty budget of the mass integration

were in agreement within these uncertainties.

CHAPTER 7

INVESTIGATION OF THE SYSTEMATIC UNCERTAINTIES

Many of the systematic uncertainties of the present experiment are identical to those determined by FRITHOF NOLTING and JÜRGEN SCHURR [20, 17, 19] in their measurement. Only a few small changes have been made in the experimental setup. Thus, only a few values of the uncertainty budget have been re-estimated. These are discussed in this chapter.

7.1 LINEARITY OF THE BALANCE

7.1.1 Upper experimental limits

As discussed in section 5.2 the amplitude of the signal was measured for approximately 230 load steps. From these values, some conclusions about the nonlinearity of the balance can be drawn. The simplest model for the nonlinearity of the balance is given by the equation

$$f(x) = \alpha x + \beta \sin\left(\frac{2\pi}{\lambda}x + \phi\right). \quad (7.1)$$

In this equation x denotes the load on the balance and $f(x)$ the output of the balance. The function $f(x)$ is called the characteristic function of the balance. In Eq. 7.1 four parameters α , β , the period λ and the phase angle ϕ are needed. For this model, the sensitivity σ of the balance changes with load. The sensitivity is

given by

$$\sigma(x) = \frac{df}{dx} = \alpha + \beta \frac{2\pi}{\lambda} \cos\left(\frac{2\pi}{\lambda}x + \phi\right). \quad (7.2)$$

This model of the nonlinearity has several advantages. Every characteristic function of the balance can be thought of as a sum of such equations with different periods λ_i . According to information from *Mettler-Toledo*, a similar balance, the AT-261 shows a sinusoidal characteristic curve. The AT-261 is a laboratory balance with a measuring range of 200 g and a resolution of 10 μ g. Engineers at *Mettler-Toledo* found a superpositions of two sine-functions with different periods in the characteristic curve of this balance. The sine-function with a period of 15 g had an amplitude of 40 μ g and that with a period of 2 g had an amplitude of 15 μ g. In addition it was found that the characteristic function was monotonic for the AT-261. This characteristic was also assumed for the balance in the present experiment. For this to be true, β has to be smaller than $\lambda\alpha/(2\pi)$.

The determination of the (small) amplitude s of the signal can be approximated by the derivative of the characteristic function according to

$$f(x+s) - f(x) \approx f(x) + s \frac{df}{dx}(x) - f(x) = s\sigma(x).$$

Thus, the amplitude of the signal $a(x)$ obeys Eq. 7.2 multiplied with the signal s . This results in

$$\hat{\sigma}(x) = A + B \frac{2\pi}{\lambda} \cos\left(\frac{2\pi}{\lambda}x + \phi\right),$$

with $A = s\alpha$ and $B = s\beta$. One way to check whether or not there is a nonlinearity in the data is to fit this function to the measured amplitudes of the signal. For a given period λ , the parameters $A(\lambda)$, $B(\lambda)$ and $\phi(\lambda)$ were obtained. In addition the sum of the squared residues, $\chi^2(\lambda)$ was calculated. To avoid a nonlinear fit, the same trick as used in section 4.2 was employed.

Two results of the fit were of particular interest. First, from $\chi^2(\lambda)$ it is possible to determine, whether the introduction of a nonlinearity improves the agreement of $y(x)$ with the data. The expectation value of the χ^2 is basically the number of degree of

freedom, assuming that the uncertainty of the individual measurements was known. Unfortunately, this uncertainty was not known. However, $\chi^2(\lambda)$ could be compared to $\chi^2(\infty)$. The value of $\chi^2(\infty)$ was obtained by fitting $y(x) = A$ to the data. With $\chi^2(\infty)$ the meaningful value $\hat{\chi}^2(\lambda) = (n - 1)\chi^2(\lambda)/\chi^2(\infty)$ could be calculated. In this equation n is the number of measurements. Obviously, this value equals the number of degrees of freedom (ν) for $(\lambda = \infty)$. Two more parameters (B and ϕ) were necessary to fit Eq. 7.2. Thus, the values of $\hat{\chi}^2(\lambda)$ for $\lambda < \infty$ should be two less than $\hat{\chi}^2(\infty)$. It should be noted that the statistical fluctuations of χ^2 is of order $\sqrt{2\nu}$. This is the standard deviation of the χ^2 -distribution. In Fig. 7.1 $\hat{\chi}^2$ is shown for a measurement with $\nu = 232$. Two negative peaks (at 10 000 μg and 20 000 μg) can be found in this figure. Nevertheless, both peaks can also be explained by statistical fluctuations. In all the data, no significant indication for a nonlinearity in the interval from 1 000 μg to 1 g was found.

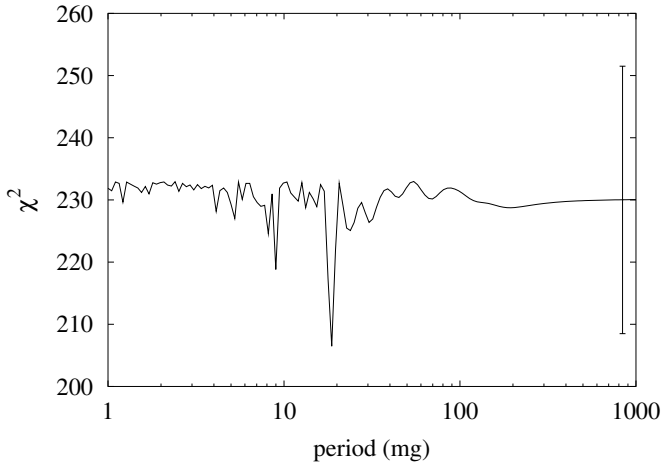


FIGURE 7.1: The $\hat{\chi}^2(\lambda)$ versus λ of the fit for a possible nonlinearity. The error bar indicates the uncertainty of χ^2 .

The other interesting result from the fit was the ratio B/A ,

which is equivalent to β/α . To understand the importance of this ratio, a small recapitulation of the averaging of the nonlinearity is needed. Using the method explained in 3.4.2 the nonlinearity of the balance was averaged out by measuring the signal at different loads. The error for the averaged signal was given by

$$\Delta s = \frac{1}{2} c_c (\delta s - s^2) f'' .$$

For the simple form of the nonlinearity given in Eq. 7.1 the value of the second derivative could be calculated using

$$f''(x) = -\beta \frac{4\pi^2}{\lambda^2} \sin\left(\frac{x}{\lambda} 2\pi + \phi\right) .$$

The absolute value of f'' was always less than $\beta 4\pi^2/\lambda^2$, which is an upper limit to estimate the error in the averaging procedure. This leads to an estimate for this error of $\delta s = 2\pi^2 c_c s (\delta - s) \beta \lambda^{-2}$. The calibration coefficient is calculated from $c_c = (b - a)/(f(b) - f(a))$. For the nonlinearity described here, the value $c_c \approx 1/a$ was a good approximation for the calibration coefficient. Therefore, the relative error of the average is of the order

$$\frac{\Delta s}{s} = \frac{2\pi^2}{\lambda^2} \frac{\beta}{\alpha} (\delta - s) . \quad (7.3)$$

For a given value of λ , the ratio β/α could be obtained from the fit. The amplitude of the signal and the spacing of the steps are known, therefore the error can be calculated. In Fig. 7.2 the ratio β/α vs. λ is shown for one measurement cycle. One sees in this figure that β/α is roughly $0.1 \mu\text{g}$. In the particular case, the highest value for this ratio is $0.18 \mu\text{g}$ for a period $\lambda = 20 \text{ mg}$. With this number, a typical value for the relative error in the signal amplitude $\Delta s/s$ is 0.044 ppm . To get this number a large value of $5 \mu\text{g}$ was used for $(\delta - s)$ in Eq. 7.3. This error is very small. Two points have to be considered. First, this is the estimated error of the nonlinearity, if the calibration device works perfectly. This means, that the signal amplitude would have been determined at equidistant load steps without any missing steps. Second, according to Eq. 7.3 the error is much larger for smaller

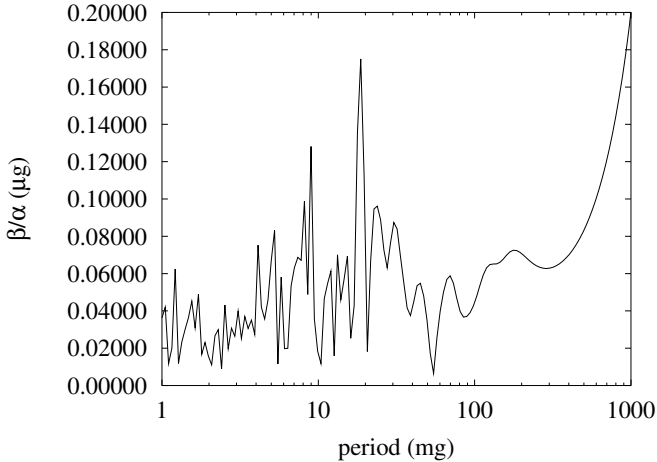


FIGURE 7.2: The fit result $\frac{\beta}{\alpha}$ versus λ .

periods λ , assuming a constant ratio β/α . The analysis of the signal amplitudes gave only values for periods larger than $2 \times 780 \mu\text{g}$. To overcome this situation and to obtain a reliable estimate of the error for the nonlinearity, several simulations were calculated.

7.1.2 Limits calculated with Monte-Carlo Simulations

In the pervious section a model of the nonlinearity of the balance was discussed. In the following simulations, the same function,

$$f(x) = \alpha x + \beta \sin\left(\frac{2\pi}{\lambda}x + \phi\right)$$

is used. The value of the parameter α cancels due to the calibration of the data. Thus, it was chosen to be one for all the simulations. The value for the ratio β/α was determined from the experimental data to be of the order of $0.1 \mu\text{g}$ for values of λ between $1000 \mu\text{g}$ and 1 g . It is reasonable to assume the same β/α , namely $0.1 \mu\text{g}$, for $\lambda < 1000 \mu\text{g}$. In the simulations, the value of the parameter λ was randomly chosen. Therefore a

uniform probability distribution of $\log(\lambda)$ in the range $1 \mu\text{g}$ and $1000 \mu\text{g}$ was assumed. For values of λ larger than $1000 \mu\text{g}$, the nonlinearity averages to zero. For values of λ smaller than $1 \mu\text{g}$ the nonlinearity averages out due to the noise of the balance, which is of order of $0.3 \mu\text{g}$. The log-distribution was a worst case assumption. In contrast to a uniform distribution in λ , the log distribution emphasized the small values of λ . As shown below, these values were more critical for the nonlinearity problem. In all, 10 000 values for λ were chosen for one simulation. It has been checked that 10 000 values gave a statistically reliable answer (at the 1 %-level). In the simulation, the correct values for the masses (CM's, TM's) and forces (gravitational forces on lower and upper TM's) were taken into account. In addition, a Gaussian noise of the balance was employed.

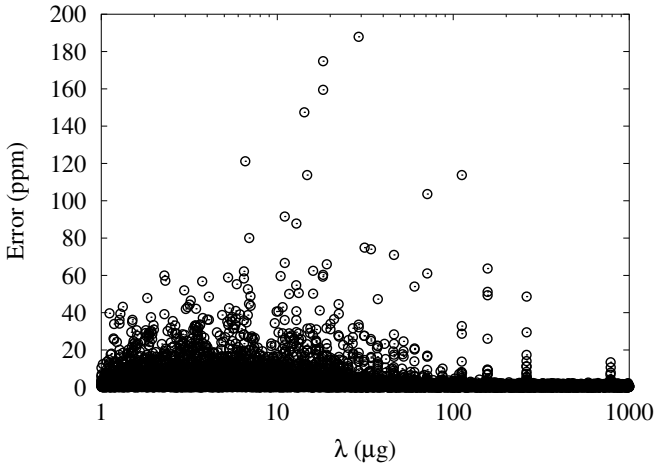


FIGURE 7.3: The remaining error of the nonlinearity as obtained by simulation. The error has both signs. In this graph, only the absolute value of the error is shown as a function of the period λ .

The result of the simulation is shown in Fig. 7.3. There exists certain values for λ where the averaging of the nonlinearity is not effective. For smaller values of λ , more of these periods occur.

However for the most values, the averaging by the calibration device works very well.

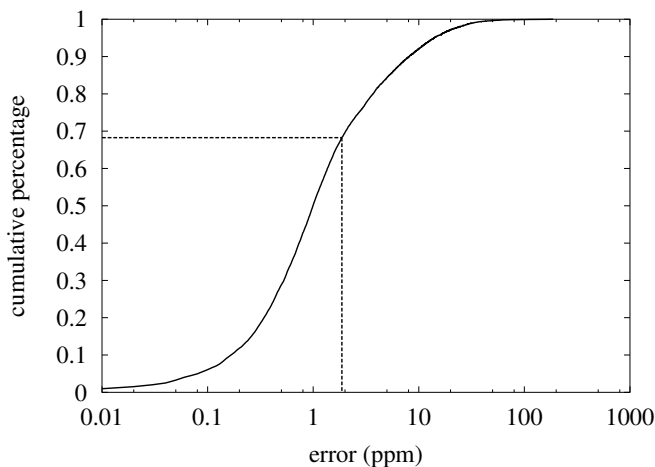


FIGURE 7.4: The cumulative percentage of the nonlinearity error, obtained by simulation.

For a given set of auxiliary weights, it is, of course, always possible to construct a characteristic curve of the balance for which a large nonlinearity error remains after averaging. The probability for such a characteristic curve has to be investigated. This was analyzed with the cumulative percentage plot. Such plot is shown in Fig. 7.4. This plot was obtained by sorting the error, obtained by the simulation (shown in Fig. 7.3) by their size. It turned out, that for 68.268 % of all simulated points, the uncertainty due to nonlinearity is smaller than 1.87 ppm.

This result was obtained under two conditions. First, it was assumed that only one sine function contributed to the characteristic function. Second, it was assumed that the calibration device worked perfectly, i.e. no missing steps occurred. To investigate the influence of these conditions, several simulations were made. The results are shown in Table 7.1. First, the dependence on the number of sine-functions in the characteristic function was

number of periods	Status of the calibration device	uncertainty (ppm)
1	works perfectly	2
2	works perfectly	4
3	works perfectly	6
4	works perfectly	9
6	works perfectly	12
10	works perfectly	18
1	only large AM's	17
6	2 successive small AM's missing	18
6	every second small AM missing	20
6	only large AM's (16 steps)	77

TABLE 7.1: Results of the simulations for various scenarios.

studied. The resulting error slowly increases with the number of sine-functions. For a characteristic function with ten different periods, the uncertainty of the averaging procedure was 18 ppm. A reasonable assumption for the number of periods was six. Six different periods in the range from $1 \mu\text{g}$ to $1000 \mu\text{g}$ are equal to a mean value of two periods per decade. No evidence of more than two periods per decade were observed. For six different periods, the influence of the malfunction of the handler was further investigated. Large parts of the data were measured with two successive missing small AM's. This leads to a total uncertainty of 18 ppm (see Table 7.1). This number applies to the measurements of the Cu series. For the Ta-I series, only the first three measurement cycles were measured with two missing small AM's. The other series were measured with the large AM's only. The results were combined to give a single results. The uncertainty of the nonlinearity were weighted according to the contribution to this number. The uncertainty due to nonlinearity of all Ta-I series together was 26.3 ppm. The measurements for the series Ta-II were basically made with every second small AM missing (e.g. the numbers 1,3,5,7,...). The uncertainty due to nonlinearity was 20 ppm (see Table 7.1).

7.2 SORPTION EFFECT

Moving the large mercury filled stainless steel tanks changed slightly the temperature of the vacuum tube. The temperature of the vacuum tube was monitored using ten semiconductor temperature sensors (National Semiconductor LM35). Several blind holes (depth approximately 5 mm) were drilled in the vacuum tube and the metallic sensors were pressed into these holes. Thus, a good thermal contact was ensured.

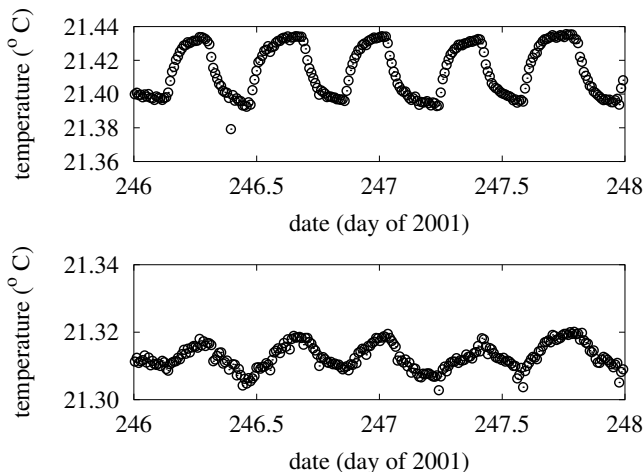


FIGURE 7.5: The measured temperature change of the vacuum tube. The upper plot shows the temperature change at the upper test mass position, the lower plot at the lower position.

The temperature was measured every ten minutes. An example of such a measurement for two days is shown in Fig. 7.5. From a more detailed analysis of the complete temperature data, the values in Table 7.2 were obtained. The values in this table give the temperature measured in FM position A minus the measured temperature in the FM position T. The temperatures were measured at the TM's positions. The temperature difference was much larger for the Cu series, than for the two tantalum series.

This was mostly due to two reasons. First, the FM position for the Ta-I series was slightly different than for the copper series. Second, during the installation of the tantalum test mass, the air flow in the lower room where the field masses were located was considerable improved.

series	temperature change		signal amplitude (ng)	uncer- tainty (ng)
	upper TM (K)	lower TM (K)		
Cu	0.040(2)	0.010(2)	-11.3	7.8
Ta I	0.004(2)	0.010(2)	-2.4	2.4
Ta II	0.014(2)	0.008(2)	-3.9	3.9

TABLE 7.2: The temperature change of the vacuum tube at the position of the test masses. At both TM positions, the vacuum tube is warmer for FM's apart. The signal amplitude column gives the estimated influence of the sorption effect on the signal amplitude. The right column is the uncertainty of this estimate.

In order to investigate the influence of the temperature on the result, additional experiments were performed. In addition to the temperature sensors, four heaters were installed on the vacuum tube. The heaters were made by simply winding resistance wire around the vacuum tube. In order to avoid a magnetic field, the winding was bifilar. The resistance of one heater was approximately 21Ω . The maximum heating power of one heater was at about 1 Watt (typically the applied voltage was 5.10 V and the current 0.24 A).

The heating was performed in such a way, that the temperature amplitude was approximately ten times larger than that of the normal measurements. During this experiment the signal amplitude was measured without using the different load steps. This was not necessary, because the influence of the nonlinearity on this measurement was negligible. The analysis of this experiment was made with the same software as used in the analysis of the real measurement data. The measured signal amplitude was scaled back to the temperature change in the normal opera-

tion. These values and their uncertainties are shown in Table 7.2. Unfortunately, the statistical noise for the measurement with the tantalum test masses was comparable to the value. However, the effect results in a negligible error for the Ta series.

7.3 MAGNETIC FORCES ON THE TEST MASSES

In this section, the magnitude of the unwanted magnetic forces on the test masses is estimated. The z-component of the magnetic force on a test mass assuming no permanent magnetization, can be calculated by

$$F = -\frac{\mu_0}{2}V\chi\frac{\partial H^2}{\partial z} , \quad (7.4)$$

where V denotes the volume of the test mass, χ is the magnetic susceptibility of the mass and H denotes the magnetic field. The susceptibility of the four test masses (two copper TM's and two tantalum TM's) were measured by RICHARD DAVIS and PHILIPPE RICHARD. The results of these measurements are shown in Table 7.3. As a side product of these measurements, the permanent magnetization was found to be zero within the measurement uncertainty (0.08 A/m). Thus, the above assumption is correct and the magnetic forces can be calculated with Eq. 7.4.

The magnetic field at the position of the test mass was measured with a fluxgate magnetometer [32]. The total measuring range of the magnetometer was $\pm 100\mu\text{T}$ with an accuracy of 0.5%. In order to measure the magnetic field, the test masses were removed and the probe was inserted into the vacuum tube on a long cable. All three field components were measured. In Figure 7.6 the absolute value of the magnetic field strength versus position is shown.

The derivative of the squared value was calculated numerically. The result of this calculation is shown in Fig. 7.7. Only the difference in the magnetic field derivative for the two field mass positions influences the weight difference. The change in the z-component of the gradient of the squared absolute value of the magnetic field strength is, in worst case, $400\text{ A}^2/\text{m}^3$. Using this value to estimate the magnitude of the magnetic force the

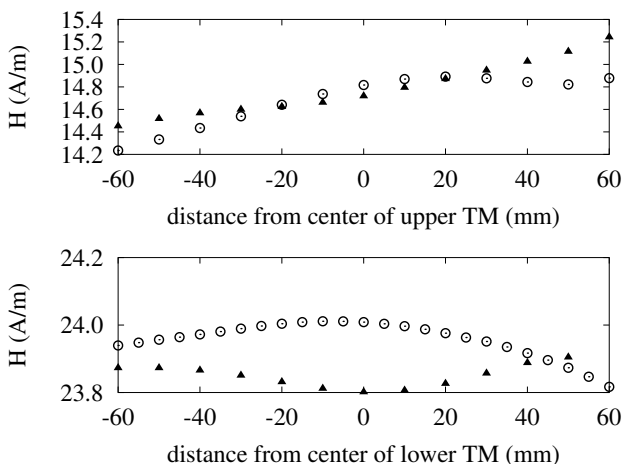


FIGURE 7.6: The absolute value of the magnetic field strength versus position. The data points indicated by circles were measured with field masses apart; those marked with triangles with field masses together.

values in Table 7.3 were obtained. These values have to be doubled for the worst case estimate of the magnetic force, involving two TM's.

	V (cm^3)	χ (10^{-6})	F (ng)	F/a (ppm)
Cu	122	4	0.01	0.01
Ta	66	191	0.32	0.41

TABLE 7.3: The magnetic force on one test mass. V denotes the volume of the main cylinder, χ the magnetic susceptibility and F the resulting force. The ratio F/a is the relative contribution to the signal amplitude.

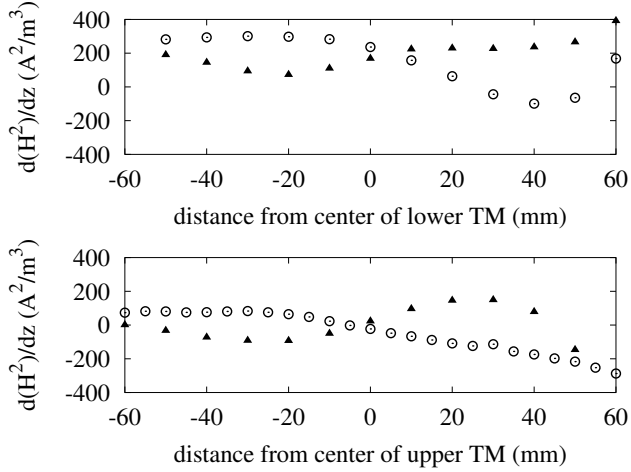


FIGURE 7.7: The derivative of the squared mean value of the magnetic field strength versus position. The circles indicate the values for field masses apart, the triangles for field masses together.

7.4 POSITION OF THE TEST MASSES

In this section, the influence of the position measurement uncertainty on the final result is discussed. The calculation of this uncertainty is obtained by straight forward error propagation. Thus, only the copper-series is shown. For the other measurement series only the end result is given.

At first, the influence of the vertical position parameters were discussed. Six heights were measured to determine the vertical positions. They were used to calculate six parameters, p_1 , p_2 , p_3 , Δ , δ and h_{sym} . This calculation introduces a correlation between different parameters. The covariance matrix of the first

five parameters, only these were used in the mass integration, is

$$V = \begin{pmatrix} 3.4 & 2.9 & 0 & 0 & 0 \\ 1.6 & 3.4 & 0 & 1.3 & 1.3 \\ 0 & 0 & 24.5 & 0 & 0 \\ -1.3 & 0 & 0 & 2.3 & 1.8 \\ 0 & 0 & 0 & 0.5 & 14.0 \end{pmatrix} \times 10^{-4} \text{ mm}^2 \quad (7.5)$$

The sensitivity of the experiment on the five parameters was calculated with the mass integration by numerically calculating the derivatives of the signal amplitude with respect to the five parameters. The results for the three different measurement series are shown in Table 7.4.

By multiplying the covariance matrix with the vector \vec{S} , containing the first derivative, one can calculate the total uncertainty of the vertical positions ($\sigma^2 = \vec{S}V\vec{S}$). The values calculated for the three measurement series are displayed in Table 7.4. In order to obtain the total position uncertainty, the vertical and horizontal position uncertainties were added quadratically. These values are summarized in Table 7.5.

series	p_1	p_2	p_3	Δ	δ
Cu	-171	57	-60	11	-23
Ta I	14	80	80	4	8
Ta II	39	210	-240	4	8

TABLE 7.4: The sensitivity of the signal amplitude on the position parameters. All values are given in ng/mm.

7.5 COMBINATION OF THE UNCERTAINTIES

For the three measurement series (Cu, Ta I, Ta II) the individual uncertainties were calculated. For the larger part of the uncertainty budget, different values were obtained for the three series (see Table 7.6). The results of the three measurements were combined to a single number. Thus, the different contributions to the uncertainty budget had to be combined.

series		Cu	Ta I	Ta II
vertical position	(ppm)	5.2	5.5	16.1
horizontal position	(ppm)	4.7	2.7	2.7
total position	(ppm)	7.0	6.2	16.3

TABLE 7.5: The relative uncertainties contributed by the position measurement.

In Table 7.6 the uncertainties for the three measurement series are shown. Four of the eleven topics of the uncertainty budget were the same for all measurements. From the remaining seven numbers, a subtotal was calculated by adding the individual uncertainties quadratically. The three values for the gravitational constants were weighted according to their subtotal. This is shown in Table 7.7.

The uncertainties were combined using the equation

$$\sigma = \left(\sum_{i=1}^3 \sum_{j=1}^3 w_i w_j \text{cov}(\sigma_i, \sigma_j) \right)^{1/2}. \quad (7.6)$$

The values w_i denote the weights of the three measurements (Cu, Ta I and Ta II). The value $\text{cov}(\sigma_i, \sigma_j)$ denotes the covariance of two of the three uncertainties. It is calculated using the correlation coefficient r_{ij} by $\text{cov}(\sigma_i, \sigma_j) = r_{ij} \sigma_i \sigma_j$. For the large part of the entries in the uncertainty budget, the correlation coefficient is one. Only for the statistical uncertainty is no correlation between the three uncertainties present. The combined uncertainty budget is calculated with the above equation. As the result of the experiment, the value for G is

$$G = (6.674\,07 \pm 0.000\,22) \times 10^{-11} \text{ m}^3 \text{ kg}^{-1} \text{ s}^{-2}.$$

source of uncertainty	contribution (ppm)		
	Cu	Ta I	Ta II
nonlinearity of the balance	18.0	26.3	20.0
position of TM's	7.0	6.1	16.3
sorption effect on TM's	10.0	3.0	5.0
statistical uncertainty	6.9	13.0	8.4
calibration weight	4.0	3.5	3.5
TM mass distribution	3.0	4.0	4.0
magnetic forces on the TM's	0.0	1.0	1.0
subtotal	23.4	30.6	28.1
FM mass distribution	20.6	20.6	20.6
numerical integration	5.0	5.0	5.0
tilt of the balance	4.0	4.0	4.0
local gravity	0.1	0.1	0.1
total	31.8	37.4	35.4

TABLE 7.6: Uncertainty budget of the final result. The last four are common to all series.

series	G	σ/G (ppm)	σ (10^{-4})	σ^{-2} (10^7)	weight w_i
Cu	6.674 04	23.36	1.559	4.114	0.4400
Ta I	6.674 10	30.60	2.042	2.398	0.2565
Ta II	6.674 08	28.12	1.877	2.838	0.3035
mean/sum	6.674 07			9.35	1.0000

TABLE 7.7: Weighted average of the three measurements. For clarity, the units of G ($10^{-11} \text{ m}^3 \text{ kg}^{-1} \text{ s}^{-2}$) were omitted.

CHAPTER 8

RESULTS AND DISCUSSION

In the final chapter, the result of the experiment along with a summary of the uncertainty budget is given. In addition, the major contributions to the uncertainty budget are briefly discussed. A comparison of the various results obtained with this experimental setup is given. Finally, the result is compared with other recently published values of the gravitational constant.

8.1 THE RESULT OF THIS WORK

During the scope of this work three measurement series, labeled Cu, Ta I and Ta II, were undertaken. The Cu series was measured with copper test masses, whereas both Ta series were made with tantalum test masses. The positions of the FM's were different in Ta I and Ta II measurement. The results of the three measurements are listed in Table 8.1. The results were combined with their uncertainties, as described in section 7.5. The resulting value of the Newtonian gravitational constant is

$$G = (6.674\,07 \pm 0.000\,22) \times 10^{-11} \text{ m}^3 \text{ kg}^{-1} \text{ s}^{-2} .$$

Thus, the relative uncertainty of the measurement is 32.8 ppm. A complete uncertainty budget for the final result is given in Table 8.2. By using the value $GM_{\oplus} = 3.986004415(8) \times 10^{14} \text{ m}^3 \text{ s}^{-2}$ as obtained by the Lageos satellite project [34], the mass of the earth could be calculated. Thus, the mass of the earth, as weighed

with the Mettler AT-1006 mass-comparator, is found to be

$$M_{\oplus} = (5.972\,37 \pm 0.000\,20) \times 10^{24} \text{ kg} .$$

	Cu	Ta I	Ta II
G ($10^{-11} \text{ m}^3 \text{ kg}^{-1} \text{ s}^{-2}$)	6.674 03	6.674 09	6.674 10

TABLE 8.1: Results obtained for the three measurement series.

source of uncertainty	contribution (parts in 10^6)
nonlinearity of the balance	20.7
position of TM's	9.6
sorption effect on TM's	6.7
statistical uncertainty	5.2
calibration weight	3.7
TM mass distribution	2.6
magnetic forces on the TM's	0.6
FM mass distribution	20.6
numerical integration	5.0
tilt of the balance	4.0
local gravity	0.1
total	32.8

TABLE 8.2: Uncertainty budget of the final result. The last four are common to all series.

8.2 REMARKS ON THE UNCERTAINTY BUDGET

The uncertainty budget of this experiment is dominated by two uncertainties, the nonlinearity of the balance and the mass distribution of the FM's. The nonlinearity contributes 20.7 ppm to the uncertainty budget. This value is a factor of ten smaller than

the estimated value given in the 1998 measurement. This reduction was achieved by determining the signal amplitude for different bias loads of the balance and averaging these values. This procedure was accomplished by the calibration device which was designed and constructed during this work. With this averaging method, it was possible to reduce the influence of the nonlinearity of the balance appreciably. It should be noted, that the small nonlinearity of the balance is not a malfunction of the balance for normal operation. The balance was primarily designed to measure 1 kg masses with a resolution of 1 μg . For this task the nonlinearity of the balance is negligible. It has been shown, that the nonlinearity is at the level of 100 ng within a range of 200 mg. In contrast, during this work, the balance was used to measure the signal amplitude of 1 mg with a relative uncertainty of 10 ppm. Nevertheless, by means of the averaging method, it was possible to achieve a reliable measurement with an uncertainty of 20.7 ppm. Is it possible to improve the uncertainty contributed by the nonlinearity? This is probably not possible by improving the averaging method. It is, however, possible by using a balance specifically designed for this purpose. Nevertheless, the time expenditure needed for this is beyond the scope of the present thesis. The second largest contribution to the uncertainty budget is the mass distributions of the FM's. One of the noteworthy properties of this experiment was the liquid field masses. On the one hand, employing a liquid as field mass ensure a uniform density. On the other hand, the need for a vessel, to fill in the liquid, was a disadvantage. This vessel is geometrically complicated, compared to the balls or cylinders used by most of the other experimental determinations of G . For the mass integration a large number of parts, like screws, O-rings, compensation vessels, outlets etc. have to be taken into account. The position, weight and dimensions of each part have to be determined and included in the mass integration. To ensure a reliable mass integration the whole software was written twice independently. From both approaches an uncertainty in the distribution of the field mass of 20.6 ppm was estimated. The other topics in the uncertainty budget were negligible, compared with the two large uncertainties, mass distribution and nonlinearity.

8.3 THE CONSISTENCY OF THE RESULTS

Before comparing this result with the results of other experiments, the internal consistency of the results should be discussed. Fig. 8.1 shows three results obtained from the series, Cu, Ta I and Ta II together with two results measured by FRITHJOF NOLTING and JÜRGEN SCHURR.

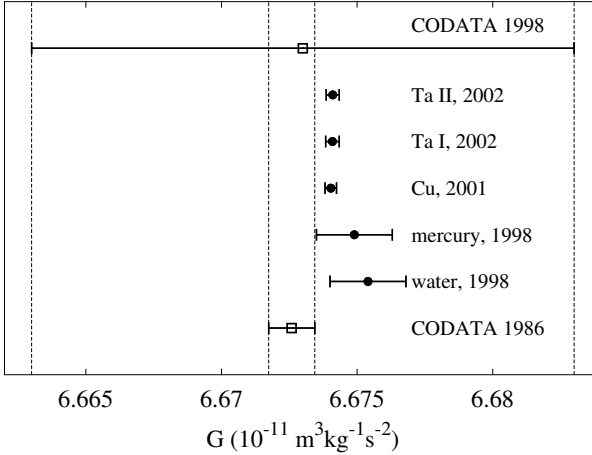


FIGURE 8.1: Comparison of all results obtained with this apparatus. The dashed lines represent the 1σ interval of the CODATA recommendation.

First, some remarks regarding the consistency of the three new results. The main difference between the copper and tantalum TM's was in the mass integration. The copper TM's were less compact than the tantalum TM's. Thus, the change in the gravitational field within the test mass has a larger influence for the copper result. The relative size of this effect, compared to the signal amplitude was approximately -4700 ppm for the copper TM's, but only -23 ppm for the tantalum TM's. The consistency of the results indicate, that the test masses have been implemented correctly in the mass integration. This consistency

check is very important for experiments of this type. Unfortunately, only in a few determinations of G by other groups such consistency checks have been made. To emphasize the importance of such checks, it should be noted that the group in New Zealand, Fitzgerald and Armstrong, performed a similar change of their test mass in 1998. They found an error in their mass integration of their 1995 experiment of approximately 1300 ppm.

In addition, the agreement of the three results is another indication for the vanishing nonlinearity of the balance. Since differences in the signal amplitude for the three measurements were at the 1000 ppm level, a significant nonlinearity would have influenced the measurements differently. Consequently the observed agreement among these three measurements is very significant.

Two values for G were measured with the same apparatus in 1998. One value was measured with water filled tanks, the second value with mercury filled tanks. The results of both measurements are shown in Fig. 8.1. Both old measured results agree with the new values within their uncertainties. This is additional evidence for the correctness of the present result. Several changes were implemented in the experiment, for example important parts of the balance has been improved. In addition, the complete software (control of the experiment, data analysis and mass integration) have been completely rewritten.

8.4 COMPARISON WITH OTHER RESULTS

Since 1998 additional new results have been published by various groups. Two results, both obtained with a horizontal torsion balance, are especial noteworthy. One experiment was made at the University of Washington (UW). Gundlach and Merkowitz [36] published in 2000 a result with a relative uncertainty of 13 ppm. The second experiment was carried out at the Bureau International des Poids et Mesures (BIPM) by Quinn and coworkers [37]. They achieved a result with a relative uncertainty of 42 ppm. The results of UW and BIPM, however, differ by more than four standard deviations. These two results and the latest results of other experiments are shown in Fig. 8.2.

The result obtained by the present work is consistent with

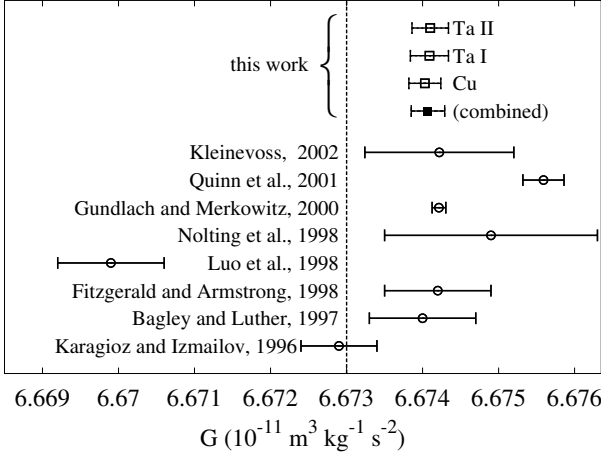


FIGURE 8.2: A comparison of recent published values of G [9, 10, 11, 13, 17, 36, 37, 38]. The outlined rectangles indicates the three results determined with different mass setups. The dashed line represents the CODATA recommendation $G = 6.673(10) \times 10^{-11} \text{ m}^3 \text{ kg}^{-1} \text{ s}^{-2}$ [2].

most of the other results. The result of PTB, is not included in Fig 8.2. There is no other result in agreement with the PTB result. Thus, it is considered to be erroneous. Only three other results do not agree with the value, obtained in the present work. The different results were the measurements carried out by Karagioz and Izmailov (2.1σ), by Luo and coworkers (5.7σ) and Quinn and coworkers (4.4σ). The number in parentheses give the deviation in units of the combined uncertainties of the corresponding result and the result presented here.

The result of this work is the determination of the gravitational constant with the second smallest uncertainty up till now. It is, however, the first result measured with a device other than a torsion balance with a relative uncertainty below 100 ppm.

BIBLIOGRAPHY

- [1] H. Cavendish, Phil. Trans. R. Soc. **88**, 469 (1789).
- [2] P.J. Mohr and B.N. Taylor, Rev. Mod. Phys. **72**, 351 (2000).
- [3] E.R. Cohen and B.N. Taylor, Rev. Mod. Phys. **59**, 1121 (1987).
- [4] K. Kuroda, Phys. Rev. Lett. **75**, 2796 (1995).
- [5] B. Hubler *et al.*, Phys. Rev. D **51**, 4005 (1995).
- [6] M.P. Fitzgerald and T. R. Armstrong, IEEE Trans. Instrum. Meas. **44**, 494 (1995).
- [7] W. Michaelis *et al.*, Metrologia **32**, 267 (1996).
- [8] H. Walesch *et al.*, IEEE Trans. Instrum. Meas. **44**, 491 (1995).
- [9] O.V. Karagioz and V.P. Izmailov, Izmeritel. Tekh. **10**, 3 (1996).
- [10] C.H. Bagley and G.G. Luther, Phys. Rev. Lett. **78**, 3047 (1997).
- [11] M.P. Fitzgerald and T. R. Armstrong, Meas. Sci. Technol. **10**, 439 (1999).

- [12] U. Kleinevoß *et al.*, Meas. Sci. Technol. **10**, 492 (1999).
- [13] J. Luo *et al.*, Phys. Rev. D **59**, 42001 (1998).
- [14] J.P. Schwarz *et al.*, Meas. Sci. Technol. **10**, 478 (1999).
- [15] S.J. Richman *et al.*, Meas. Sci. Technol. **10**, 460 (1999).
- [16] F. Nolting *et al.*, Meas. Sci. Technol. **10**, 439 (1999).
- [17] F. Nolting, Ph.D. thesis, Universität Zürich (1998).
- [18] A. Cornaz *et al.*, Physik-Institut Universität Zürich, Wissenschaftlicher Jahresbericht 1994/95.
- [19] J. Schurr *et al.*, Phys. Rev. Lett. **80**, 1142 (1998).
- [20] J. Schurr *et al.*, Phys. Lett. A **248**, 295 (1998).
- [21] Reissbühler AG, Wallisellen, Switzerland.
- [22] H. Stöcker, Taschenbuch der Physik, Harri Deutsch, Frankfurt/Main, 1994.
- [23] Laser Tracker 500, Leica.
- [24] H. Bettin and H. Krumscheid, Metrologia **36**, 547 (1999).
- [25] PTB-Stoffdatenblätter, Mercury, SDB-12, PTB. (1999).
- [26] private communication Jean-Luc Pochon, PSI.
- [27] TC2002, Leica.
- [28] Linear Scale Unit AT112, Mitutoyo.
- [29] private communication Martin Baumeler, metrotec.
- [30] T. J. Quinn, Meas. Sci. Technol. **3**, 141 (1992).
- [31] private communication Eugen Holzschuh.
- [32] MAG-03MC From Bartington Instruments Ltd, Oxon, England.

- [33] R. Davis, J. Res. Natl. Inst. Stand. Technol. **100**, 209 (1995).
- [34] J.C. Ries *et al.*, Geophys. Res. Lett. **19**, 529-531 (1992).
- [35] private communication Philippe Richard, metas.
- [36] J.H. Gundlach and S.M. Merkowitz, Phys. Rev. Lett. **85**, 2869 (2000).
- [37] T.J. Quinn *et al.*, Phys. Rev. Lett. **87**, 111101 (2001).
- [38] U. Kleinevoß , Ph.D. thesis, University Wuppertal, **WUB-DIS 2002-2**.

ACKNOWLEDGMENTS

This thesis was only possible with the support of many people to whom I would like to express my gratitude.

The work was carried out at the Physics Institute of the University of Zürich. PROF. DR. WALTER KÜNDIG was my first supervisor. He was the father and inventor of this experiment. I would like to thank him for the challenging opportunity to finish this work. Even after his retirement in 1999, he was highly engaged and gave me a major motivation to carry on.

DR. EUGEN HOLZSCHUH joined the group in 1999. He died unexpectedly in November 2001. This excellent experimental physicist contributed major ideas to the experiment. I am very grateful to having had the opportunity of working with this brilliant physicist. I will always remember the informal and challenging talks about various physics topics in the coffee breaks.

After becoming an orphan (sole member of the gravitational group), PROF. ULRICH STRAUMANN and PROF. HUGO KELLER gave me the chance to continue my work under their supervisions. They spent many hours reading publications and discussing delicate details of the uncertainty analysis. I would like to thank both for their support and their confidence in my work.

In the last month of intense thesis writing, DR. R. E. PILEY supported me extraordinarily. He was there to discuss my personal and scientific problems in a most tolerant way. His wise suggestions and clear point of view gave me support in many ways. I am greatly indebted to him.

The experiment was set up by DR. FRITHJOF NOLTING and DR. JÜRGEN SCHURR. Both introduced me to the experiment with much patience. Even after they left Zürich, they answered my questions and were interested in the ongoing experiment. I would like to thank them for their great work and support. I am particularly impressed by the precision with which they filled the tanks with mercury.

DR. PHILIPPE RICHARD from the national metrology institute of Switzerland (metas) measured various masses and densities. I would like to thank him for his prompt and precise service.

DR. HORST BETTIN from the national metrology institute of Germany (PTB) measured the mercury density. I thank him for his precise measurements.

MARKETA MALINA from Mettler Toledo determined the mass of the test masses several times. It was always nice to be at Mettler Toledo in her company. I would like to thank her for all of the measurements and discussions.

I would also like to thank MARTIN BAUMELER and his staff at the company Metrotec for modifying the balance and constructing the calibration device. His design hints were most valuable.

In addition, I would like to thank ULI FEHLMANN and JEAN-LUC POCHON for the position measurements.

Besides myself, three people took responsibility for the handling of the mercury. DR. A. FEICHTINGER and JÖRG FRANK from the University Zürich and G. COZZATTI from PSI. I would like to thank them for their advice and tips regarding safety, as well as their control measurements.

I would like to thank the following people from the university for various help and support: BERNHARD SCHMID and his staff, WALTER FÄSSLER, LUCIEN PAULI, JÜRG SEILER, TIZIANO CRUDELI and ROSMARIE RÖSSEL.

Finally, I want to express my gratitude to my wife MONIKA for her patience and support during the last four years.

LEBENS LAUF

PERSONALIEN

Name	Schlamminger
Vorname	Stephan
Geboren	am 18.06.1973 in Kelheim
Staatsangehörigkeit	deutsch

AUSBILDUNG

1983 – 1992	Donaugymnasium Kelheim
1993 – 1998	Studium der Physik an der Universität Regensburg
1998	Diplom in Physik
Titel der Diplomarbeit	Charakterisierung kristallographischer und elektrischer Eigenschaften von Hoch-Epsilon- Dielektrika.
1998 – 2002	Wissenschaftlicher Mitarbeiter und Assistent am Physik Institut der Universität Zürich bei Prof. U. Straumann und Prof. H. Keller unter deren Leitung die Dissertation erstellt worden ist.